Exploration of fMRI brain responses to oral sucrose after Roux-en-Y gastric bypass in obese yucatan minipigs in relationship with microbiota and metabolomics profiles

Damien Bergeat, Nicolas Coquery, Yentl Gautier, Sarah Clotaire, Émilie Vincent, Véronique Romé, Sylvie Guerin, Isabelle Le Huërou-Luron, Sophie Blat, Ronan Thibault, et al.

Clinical Nutrition 42 (2023) 394–410

Contents lists available at ScienceDirect

Clinical Nutrition

journal homepage: http://www.elsevier.com/locate/clnu

Original article

Exploration of fMRI brain responses to oral sucrose after Roux-en-Y gastric bypass in obese yucatan minipigs in relationship with microbiota and metabolomics profiles

Damien Bergeat [a, b], Nicolas Coquery [a], Yentl Gautier [a], Sarah Clotaire [a], Émilie Vincent [a], Véronique Romé [a], Sylvie Guérin [a], Isabelle Le Huërou-Luron [a], Sophie Blat [a], Ronan Thibault [a, c, **], David Val-Laillet [a, *]

[a] Inrae, Inserm, Univ Rennes, Nutrition Metabolisms and Cancer, NuMeCan, Rennes, St Gilles, France
[b] Department of Digestive Surgery, CHU Rennes, Rennes, France
[c] Department of Endocrinology-Diabetology-Nutrition, Home Parenteral Nutrition Centre, CHU Rennes, Rennes, France

ARTICLE INFO

Article history:
Received 26 July 2022
Received in revised form
6 January 2023
Accepted 19 January 2023

Keywords:
Obesity
Gastric bypass
Bariatric surgery
Microbiota
Brain
Functional MRI

SUMMARY

Background & aims: In most cases, Roux-en-Y gastric bypass (RYGBP) is an efficient intervention to lose weight, change eating behavior and improve metabolic outcomes in obese patients. We hypothesized that weight loss induced by RYGBP in obese Yucatan minipigs would induce specific modifications of the gut–brain axis and neurocognitive responses to oral sucrose stimulation in relationship with food intake control.

Methods: An integrative study was performed after SHAM (n = 8) or RYGBP (n = 8) surgery to disentangle the physiological, metabolic and neurocognitive mechanisms of RYGBP. BOLD fMRI responses to sucrose stimulations at different concentrations, brain mRNA expression, cecal microbiota, and plasma metabolomics were explored 4 months after surgery and integrated with WGCNA analysis.

Results: We showed that weight loss induced by RYGBP or SHAM modulated differently the frontostriatal responses to oral sucrose stimulation, suggesting a different hedonic treatment and inhibitory control related to palatable food after RYGBP. The expression of brain genes involved in the serotoninergic and cannabinoid systems were impacted by RYGBP. Cecal microbiota was deeply modified and many metabolite features were differentially increased in RYGBP. Data integration with WGCNA identified interactions between key drivers of OTUs and metabolites features linked to RYGBP.

Conclusion: This longitudinal study in the obese minipig model illustrates with a systemic and integrative analysis the mid-term consequences of RYGBP on brain mRNA expression, cecal microbiota and plasma metabolites. We confirmed the impact of RYGBP on functional brain responses related to food reward, hedonic evaluation and inhibitory control, which are key factors for the success of anti-obesity therapy and weight loss maintenance.

1. Introduction

Roux-en-Y gastric bypass (RYGBP) is presently the reference procedure for surgical management of obesity, sustaining long-term weight loss [1], resolving diabetes and its long-term complications [2], and increasing patients' survival [1]. The metabolic outcomes of this surgery have been demonstrated in different species including humans, minipigs and rodents. Key features of the metabolic improvement encompass modulations of the pancreatic β-cell function, incretin (*e.g.* Glucagon-like peptide-1 [GLP1]) and satiety hormones secretion involved in glucose homeostasis, as well as biliary acid signaling [3]. Also, the gut microbiota dysbiosis documented in the context of obesity [4,5] seems to be reduced after weight-loss surgery in some studies [6], possibly contributing to the resolution of metabolic disorders [7].

* Corresponding author.
** Corresponding author. Inrae, Inserm, Univ Rennes, Nutrition Metabolisms and Cancer, NuMeCan, Rennes, St Gilles, France
E-mail addresses: ronan.thibault@chu-rennes.fr (R. Thibault), david.val-laillet@inrae.fr (D. Val-Laillet).

https://doi.org/10.1016/j.clnu.2023.01.015

List of abbreviations

5HT2B	5-Hydroxytryptamine (Serotonin) receptor 2 B
Ac	nucleus accumbens
AGC	Automatic gain control
AgRP	Agouti Related Neuropeptide
AIF1	Allograft Inflammatory Factor 1
AMY	amygdala
A-PFC	anterior prefrontal cortex
AU	arbitrary units
BDNF	Brain derived neurotrophic factor
BLAST	Basic Local Alignment Search Tool
BOLD	blood-Oxygen-Level Dependent
CART	Cocaine and amphetamine regulated transcript protein
CB1	Cannabinoid receptor 1
CCKBR	Cholecystokinin B receptor
Cd	caudate nucleus
CREEA	Rennes Committee of Ethics in Animal Experimentation
DDA	Data-dependent analysis
DL-PFC	dorsolateral prefrontal cortex
DP-CC	dorsal posterior cingulate cortex
EPI	Echo-planar imaging
FEW	family wise error
fMRI	functional magnetic resonance imaging
FWHM	full width half maximum
F/B	Firmicutes/Bacteroidetes ratio
GLP1	Glucagon-like peptide-1
GLP1	R Glucagon like peptide receptor 1
HRLC	high resolution liquid chromatography
HTR1a	5-Hydroxytryptamine Receptor 1 A
HTR1F	5-Hydroxytryptamine Receptor 1 F
HYP	hypothalamus
IC	insular cortex
IL1bR	Interleukin 1 Beta receptor
LC-HRMS	Plasma Liquid Chromatography High Resolution Mass Spectrometry
LEPR	Leptin receptor
MANOVA	Multivariate analysis of variance
MCT1	Monocarboxylate Transporter 1
MP-RAGE	Magnetization-prepared rapid gradient-echo
MW	metabolic weight
NFT3	Neurotrophin 3
NPYY	Neuropeptide Y receptor Y2
NCE	normalized collision energy
NPY	Neuropeptide Y
OCLN	Occludin
OFC	orbitofrontal cortex
OPLS-DA	orthogonal supervised partial least-squares-discriminant analysis
OTU	Operation Taxonomic Units
PCA	principal component analysis
PDGFRB	Platelet-derived growth factor receptor B
PET	positron emission tomography
PFC	prefrontal cortex
POD	postoperative day
POMc	Proopiomelanocortin
PP	prepryriform area
Put	putamen nucleus
QC	Quality control
RINS	insulin receptor
ROIs	Region of interest
RYGBP	Roux-en-Y gastric bypass
SCFA	short-chain fatty acid
SLC27A1	Long-chain Fatty Acid Transport Protein 1
STD	standard diet
SVC	small volume correction
TLR4	Toll-like receptor 4
TNFα	Tumor necrosis factor alpha receptor 1
TR/TE	Reception time/Echo time
VIP	variable importance projection
VTA	ventral tegmental area
WGCNA	weighted (gene) correlation network analysis
W4M	Workflow4Metabolomics
ZO1	Zonulin 1

In humans, RYGBP can also effectively change eating behavior, and notably the hedonic evaluation and consumption of palatable foods associated with negative health outcomes. Several studies used functional magnetic resonance imaging (fMRI) and nuclear imaging (positron emission tomography, PET) to explore brain activity, neurotransmission and metabolism [8,9]. In humans, hedonic responses to food pictures were found modulated in the mesolimbic and frontostriatal circuits after RYGBP [10,11]. The complex reprogramming of eating behavior following RYGBP can be considered as one of the key factors of the global success of the treatment. Understanding which factors and markers are involved in the RYGBP-induced modifications of the microbiota–gut–brain axis is necessary to disentangle the complex interactions between organs and processes ultimately leading to modifications of eating habits. This knowledge would be valuable to disentangle the physiological and metabolic mechanisms of RYGBP, but also to conceive less invasive alternative treatments for morbid obesity and its comorbidities. To our knowledge, studies combining and integrating data from the microbiota, gut and brain with the aim to document the effects of RYGBP at a systemic level are very scarce or inexistent. A validated analytical procedure such as weighted correlation network analysis (WGCNA) [12] is a powerful tool to integrate different large datasets and elaborate hypotheses linking different factors (*e.g.*, microbiota and plasma metabolites) associated with surgery type and functional responses.

The present study aimed at investigating in obese minipigs, a pertinent preclinical model for nutrition and neurosciences research, the consequences of weight loss, induced either by RYGBP or SHAM surgery combined with a pair-feeding procedure, on brain functions, microbiota composition and metabolomic profiles. We hypothesized that weight loss induced by RYGBP compared to restrictive diet only would be associated with specific modifications of the microbiota–gut–brain axis, and especially: i) significant variations of the microbiota composition and plasma metabolome profiles, ii) modulation of the expression of genes in key brain regions of interest (ROIs) involved in reward, motivation and cognition, and finally iii) different neurocognitive Blood-Oxygen-Level Dependent (BOLD) fMRI brain responses to the oral perception of sucrose that usually triggers specific activations of the corticostriatal circuit.

2. Materials and methods

2.1. Ethics

The experiments presented in this paper were conducted at the INRAE center of St Gilles, France (Agreement No 3527532) and in accordance with the current ethical standards of the European Community (Directive 2010/63/EU). This protocol was approved by the local Ethics Committee CREEA (Rennes Committee of Ethics in Animal Experimentation) (authorization #201504280924565) and the Ministry of Higher Education and Research (Reference No APAFIS #598–201 504 280 924 565 v5).

2.2. Animals and housing

The choice of the minipig model to study the complex reprogramming of eating behavior following RYGBP is supported by a large bundle of arguments at different levels: i) Minipigs share close similarities with the human in terms of intestinal physiology and metabolism [13,14], ii) obese minipigs present similar basal brain metabolism anomalies as those observed in obese humans [15], iii) several research groups have already reported studies using RYGBP model [16] in minipigs, even in the obese condition [17], and iii) we already demonstrated that RYGBP in obese Yucatan minipigs can modulate basal brain responses using PET imaging [18]. Finally, our team has already designed and published a protocol to investigate BOLD fMRI brain responses to gustatory food stimulation in the minipig model [19].

Sixteen 2 years Yucatan minipigs (sex ratio = 0.5 in each group) were kept in a room of 50 m^2, maintained at a temperature of 22 °C and equipped with artificial lighting with a 15:9 light/dark cycle. As soon as they entered the experiment, the animals were housed in individual pens measuring 0.88 m^2 in surface and 1.10 m in height, with bars allowing contact between animals in adjacent pens. Each animal had access to water *ad libitum*, and had a metal chain to play.

2.3. Design of the study (Fig. 1)

In order to study the specific effect of the RYGBP in obese Yucatan minipigs without any food intake bias, we compared the RYGBP procedure with a SHAM surgery combined with a pair-feeding strategy. This procedure guaranteed similar energy intake and nutrient supply in both groups, with the hypothesis/aim to trigger similar weight loss but different effects and adaptation mechanisms of the microbiota–gut–brain axis. At the central level, BOLD fMRI brain responses to oral sucrose perception were mapped in anaesthetized animals and differential mRNA expression in brain ROIs was investigated post-mortem. At the peripheral level, cecum microbiota and plasma metabolomic analyses were performed. Multi-omic analysis strategy was used to integrate these data from various sources.

The procedures for housing, feeding, induction of obesity and surgery were identical to those described in our previous paper with the same animals (Gautier et al., 2020).

2.4. Induction of obesity

Before induction of obesity, and as routinely done in our department, animals were fed with a standard diet at 0.30 MJ/kg MW/day (where MW = Body Weight$^{0.75}$ represents the metabolic weight). Obesity was then induced in 16 lean adult Yucatan minipigs with an obesogenic diet consisting in *ad libitum* high-fat and high-sugar diet (10.8 MJ/kg) (Sup. Table 1) during at least 6 weeks [15]. Due to potential serious side effects of massive weight gain, the animals were rationed from the 15th week of obesogenic diet (when the 60% excess weight was reached) according to a gradual restriction plan (please see Gautier et al., 2020 for justifications) [18].

2.5. Weight loss interventions

Weight loss was obtained using two different approaches: Obese minipigs were homogeneously allocated (by sex, body weight, and original batch in reference to Gautier et al., 2020) to the groups RYGBP (n = 8) or SHAM surgery with pair-feeding (n = 8) groups. In the first group, a classical RYGBP was performed (see below) while, in the second, a sham surgery was performed to avoid the confounding effect inherent to the surgery (i.e. anesthesia, antibioprophylaxis, analgesia, and the stress induced by the intervention). To investigate the specific effects of RYGBP minimizing the confounding effect of weight loss, all animals were subjected to a restrictive diet in a pair-feeding plan calculated according to the consumption in RYGBP group.

2.6. Protocols of anesthesia, surgery and postoperative care

All surgeries were conducted under general anesthesia by laparotomy after an overnight fast. Anesthesia was induced by an intramuscular injection of ketamine (5 mL/kg Imalgene 1000, Merial, Lyon, France) and maintained during surgery with isoflurane inhalation (Aerane 100 mL, Baxter SAS, France). Artificial ventilation was performed after tracheal intubation with a frequency at 15 breathing/min, tidal volume between 420 and 470 mL, and spCO2 lower than 5%. Pain management was assured with intravenous injection of morphine at 0.4 mL/min (Fentanyl Renaudin 50 μg/mL). Vascular filling was ensured with Ringer Lactate drip at 22 mL/min (Braun Medical).

All surgeries were performed by DB, a senior surgeon with a regular clinical practice in obesity surgery. In the RYGBP group, a classical RYGBP was conducted to reproduce the human model with a 150-cm alimentary limb, a 70-cm biliary limb, and a small gastric pouch (30 mL) with a calibrated gastrojejunal anastomosis, as described previously [17]. Both gastrojejunal and jejunojejunal anastomoses were hand-sewn with a 4.0 absorbable running suture. Mesenteric defects were systematically closed. In the SHAM group, a laparotomy was performed and the intestine was handled during at least 20 min before closing the laparotomy.

After surgery, pain management was ensured by subcutaneous injection of morphine (0.5 mg/kg of body weight, Morphine Chlorhydrate Renaudin, lab. Renaudin – 64 250 Itxassou, France). Antibioprophylaxis using intramuscular injection of amoxicillin at 15 mg/kg BW (Dufamox LA, Zeotis, 75 014 Paris, France) was performed the day of the surgery and two days later.

Diet recovery was adapted from the postoperative protocol used in humans operated from RYGBP. Water intake was allowed the night of the surgery and an exclusive mixed standard diet was offered during three weeks before returning to a standard diet (7.27 MJ/kg) based on feed pellets at one month. The reintroduction of food after surgery was done gradually to reach 500 g/day (3.635 MJ/day) in the RYGBP group at postoperative Day 5 (POD5). To limit stress and discomfort, SHAM animals were offered a standard diet (STD) soup up to 100 g even in the case of a complete feed rejection in RYGBP animals in the first postoperative days. The ration in the SHAM group was adjusted monthly to match the RYGBP consumption. Daily surveillance by staff members was ensured to appreciate the animals' general condition as well as to control pain and food tolerance. All animals were weighed once a week and food intake was monitored daily.

A few days before euthanasia, plasma samples (on heparin) were collected in fasted animals and stored at −80°c for metabolomic analyses.

2.7. Functional imaging

2.7.1. Anesthesia

Anesthesia and animal monitoring were performed as already described [19–22]. Briefly, initial sedation was performed with an intramuscular injection of ketamine (5 mg/kg − Imalgene 1000, Merial, Lyon, France) on overnight-fasted animals. Isoflurane inhalation (Aerane 100 mL, Baxter SAS, France) was used to suppress the pharyngotracheal reflex and then establish a surgical level of anesthesia, 3–5% (less than 5 min) and 2.5–3% respectively. After intubation, anesthesia was maintained with 2.5–3% isoflurane. Cotton wool with an additional headset were used to conceal the animal's ears, and tape was used to maintain the eyes closed.

2.7.2. Gustatory stimulation

A computer-controlled apparatus (i.e., gustautomat) was used to provide gustatory stimulation to anesthetized animals as described in a previous paper implementing brain nuclear imaging in the pig model [23] and further adapted for fMRI setup [19]. Sucrose (5 and 15%, S/8560/65, Fisher Chemical, Leics, United Kingdom) was solubilized in artificial saliva [24]. Three blocks of stimulation were performed from the least to the most concentrated solution in mouth: Control stimulation with artificial saliva (i.e., 0% sucrose), sucrose 5% stimulation, and sucrose 15% stimulation. Each stimulation was repeated 15 times and consisted in oral stimulation (5 s, 24 mL/min), 25-s pause, rinse with artificial saliva (15 s, 24 mL/min), and pause (15 s). Continuous oral suction via a toric tube positioned on the tongue was applied simultaneously to the sucrose stimulation in order to flush the overflow in the oral cavity and avoid passive ingestion. There was consequently no sucrose stimulation of the digestive tract below the mouth. The entire BOLD fMRI protocol lasted about 1 h.

2.7.3. MRI image acquisition

Image acquisition was performed as previously described [19–21] on a 1.5-T magnet (Siemens Avanto) at the *Rennes Platform* for Multimodal Imaging and Spectroscopy (PRISM AgroScans, Rennes, France). *T1 weighted anatomical image acquisition*: A magnetization-prepared rapid gradient-echo (MP-RAGE) sequence was adapted to the adult minipig anatomy (160 slices, $1.2 \times 1.2 \times 1.2$ mm^3, NA = 2, TR = 2400 ms, TE = 3.62 ms, TI = 854 ms, FA = 8°). *BOLD signal acquisition*: An echo planar imaging sequence was adapted to pig head geometry (32 slices, reception time/echo time (TR/TE): 2500/40 ms, FA: 90°, voxel size: $2.8 \times 2.8 \times 2.8$ mm^3). The field of view was of 180×180 mm, the matrix size was 64^2, and the total echo-planar imaging (EPI) time was 32 min 30 (780 volumes x 2.5 s/volume, 4 initial volumes as dummy scans).

2.7.4. Data processing and statistical image analysis

Data analysis was performed with SPM12 (version 6906, Wellcome Department of Cognitive Neurology, London, UK) as previously described [21,22]. *Voxel-based statistic*: first-level (within-individual contrast) and second-level (within-group contrast) statistics were assessed with a threshold set at $P < 0.05$ to produce the brain maps of activation. *Small Volume Correction (SVC)-based statistics*: twelve anatomical ROIs corresponding to six bilateral brain structures previously studied in Gauthier et al. [18] were used: nucleus accumbens (Ac), caudate nucleus (Cd), putamen (Put), orbitofrontal cortex (OFC), and anterior and dorsolateral prefrontal cortex (A-PFC and DL-PFC). They were studied with a P-value corrected with a Bonferroni correction at a threshold of 0.05 (peak level). The related uncorrected P-value threshold after Bonferroni correction was 0.0042. For voxel- and SVC-based statistics, some suprathreshold voxels were detected with Family Wise Error (FWE) correction at $P < 0.05$. *ROI-based statistics for multiple comparison*: for multivariate analysis the parameter estimates for each contrast were measured in four brain structures corresponding to the same brain structures isolated for mRNA expression analysis, i.e. left hippocampus, left striatum (Cd and Put), the prefrontal lobe and the hypothalamus (HYP). In the manuscript, for the sake of simplification, the terms “brain responses” stand for “fMRI BOLD responses” and the qualificatives “higher” or “lower” are used to describe significant differences in brain responses between groups or conditions.

2.7.5. Euthanasia and tissue sample

Four months after surgery, all minipigs were euthanized by electrical stunning and exsanguination. After euthanasia, we performed a prompt revision of the laparotomy allowing access to the abdominal cavity and content. The cecum content was collected and immediately immersed in liquid nitrogen before being stored at −80 °C. At the same time, the brain was extracted and four regions of interest were sampled, including the bilateral prefrontal lobe as well as the entire HYP, the left hippocampus and striatum. Brain samples were promptly frozen in liquid nitrogen before being stored at −80 °C.

2.8. Brain mRNA expression analysis

2.8.1. RNA extraction and high-throughput quantitative PCR (HT-qPCR)

Total RNA was extracted from 100 mg of frozen tissue from the four brain ROIs with phenol/chloroform treatment followed by silica membrane purification (Qiagen, Hilden, Germany). Extracted RNAs were quantified using a DeNovix spectrophotometer (Wilmington, USA) and the RNA quality and integrity were confirmed using the Agilent RNA 6000 Nano kit utilizing Agilent 2100 Bioanalyzer (Agilent Technologies France, Massy, France). cDNA was prepared by reverse transcription of 2 μg total RNA using a High Capacity Complementary DNA Reverse Transcription Kit according to the manufacturer's instructions (Applied Biosystems, Foster City, CA, United States).

To evaluate the relative mRNA expression of targeted genes in samples, high-throughput quantitative PCR (HT-qPCR) was performed using the Smartchip Real time PCR technology using the Wafergen Smartchip cycler and Smartchip Multisample Nanodipenser (Biogenouest Genomics and the Human & Environmental Genomics core facility of Rennes, Rennes, France). A total of 80 primer sets were used including 13 genes selected as housekeeping genes (Sup. Table 2). Primer sets were either selected from the literature or designed using primer blast. For each brain ROIs (i.e., hypothalamus, hippocampus, striatum and prefrontal cortex), the selected housekeeping genes were both the most stable genes among the 13 housekeeping genes tested as considered by the Normfinder algorithm [25], and the housekeeping genes that were not affected by the surgical treatment (no statistical differences between RYGBP and SHAM groups). Relative expressions of the target genes were determined using the $2^{-\Delta\Delta Ct}$ method.

2.8.2. Fermentation activity assessment

The fermentation activity of the intestinal microbiota was assessed (before surgery, at 2 and 6 weeks after surgery and at sacrifice) through the quantitative analysis of short-chain fatty acids (SCFA) in feces. Fecal samples were stabilized with 0.5% orthophosphoric acid at a rate of 1 mL acid/g feces. After

centrifugation at 1700 g for 15 min at 4 °C, 1 mL of supernatant by sample was stored at −20 °C before SCFA measurement using gas chromatography analysis as previously reported [26].

2.8.3. Cecum microbiota analysis

The total cecum DNA was extracted and then sequenced as described by Anathar et al. [27]. Amplification of bacteria DNA was realized using 5′ ACGGRAGGCAGCAG et 3' AGGATTAGATACCCTGGTA primers. Sequencing was performed at the Genotoul GeT-PlaGe, Toulouse, France using Illumina MiSeq technology. The 16 S rRNA sequences were managed with FROGs (Find Rapidly OUT with Galaxy Solution), a bioinformatic pipeline. Quality control depletions conserved amplicon between 380 and 500 bp, sequences with ambiguous bases and sequences that did not contain good primers. Swarm was used to perform clustering with an aggregation maximal distance of 1 base [28]. Affiliation was performed using the Silva 16 S database and NCBI Basic Local Alignment Search Tool (BLAST). Manual annotation completed the initial affiliation in case of bad annotation or multi affiliation.

Phyloseq package was used for analysis. Operation Taxonomic Units (OTUs) found in less than 3 samples and whose abundance was less than 5.10^{-5}% were eliminated. Sample depth was normalized using GMPR [29]. Alpha diversity indexes and beta diversity indexes (Bray Curtis and Weighted UniFrac distance between samples) were calculated. Multivariate analysis of variance (MANOVA) was performed using Adonis function with 999 permutations. To identify differential abundance of OTUs between RYGBP and SHAM surgery, DESeq2 was used [30]. No material was available for one animal in the RYGBP group because of sequencing failure due to poor sample quality.

2.9. Plasma liquid chromatography high resolution mass spectrometry (LC-HRMS) based metabolomic analysis

2.9.1. Plasma sample preparation

Plasma samples (30 μL) have been extracted following the Bligh and Dyer method [31]. Blank (water) and quality control (QC) (pooled aliquot of the 32 plasma samples) were also prepared.

2.9.2. Analytical platform

Plasma metabolome analyses were performed using an Ultimate series high resolution liquid chromatography (HRLC) system coupled to a Q Exactive™ Orbitrap type high-resolution mass spectrometer (Thermo Fisher Scientific, Bremen, Germany) through a heated electrospray ion source (HESI-II, ThermoFisher Scientific). External mass detector calibration was performed before each batch by infusing calibration mixture for negative and positive ionisation mode (MSCAL6 and MSCAL5 ProteoMass LTQ/FT-Hybrid, Supelco, Bellefonte, PA, USA). Instrument was controlled by Xcalibur (ThermoFisher Scientific) software version 2.3.

2.9.3. Liquid chromatography settings

Compound separation was performed using a Hypersil GOLD-C18 column (1.9 μm, 100 mm × 2.1 mm) from Thermo-Scientific (USA). The column temperature was set at 35 °C. The mobile phases were composed of 0.1% of acetic acid in water (solvent A) and in acetonitrile (solvent B). The applied gradient (A:B, v/v) was as follows: 95:5 from 0 to 2.4 min, 75:25 at 4.5 min, 25:75 at 11 min, 0:100 from 14 at 16.5 min and 95:5 from 19 to 25 min. The flow rate was set to 0.40 mL/min. The injection volume was 5 μL. All samples were analyzed in one batch without any stopping or recalibration step. A same QC sample (mix of all samples) was injected regularly throughout the run after every five samples to monitor the stability of system. A random injection order was used to avoid confounding effects in case of signal drift during MS acquisition.

2.10. MS and MS/MS settings

2.10.1. Full MS mode

Q Exactive Orbitrap MS was operated in switching positive and negative electrospray ionization modes (ESI+ and ESI- respectively). Data were acquired in full scan mode over the mass-to-charge ratio (m/z) range 65–975 at a resolving power of 70 000 full width half maximum (FWHM) at m/z 200. Automatic gain control (AGC Target) was set at 1.10^6 and maximum injection time (IT) at 100 ms. Parameters were: Sheath gas flow, 55 arbitrary units (AU); Auxiliary gas flow, 10 AU; Capillary temperature, 350 °C; Heater temperature, 300 °C; S-lens radio frequency, 40 AU. Spray voltage was set at 3.0 kV.

2.10.2. Data-dependent analysis (DDA) mode

For annotation purpose, iterative data dependent MS/MS experiments were run on QC pool samples (iterations = 3). Iterative exclusion lists were created with IE-Omics R script. In brief, for DDA measurements, a duty cycle consisted of a full scan acquisition, followed by a TopN MS/MS (MS2) data dependent fragmentation event, taking the 3 most abundant ion species not on the dynamic exclusion list. Blank samples injections were used to create the initial positive mode and the negative mode exclusions lists. For the 3 iterative injections, a new Top 3 DDA the exclusion list was updated with IE-Omics script. For every iterative DDA measurement, two injections of samples were done to cover both polarities. The full MS1 events were acquired over the mass-to-charge ratio (m/z) range 65–975 at a resolving power of 70 000 FWHM at m/z 200. Automatic gain control (AGC) target was set at 1.10^6 and maximum injection time (IT) at 120 ms. Other parameters were the same as for the full MS mode experiments. The Top 3 MS/MS events were acquired in profile mode at 17 500 resolution using 1 microscan, an AGC target of 10^5, a maximum injection time of 80 ms, an isolation window of 1.0 m/z, an isolation offset of 0.0 m/z, a stepped normalized collision energy (NCE) (HCD) mode combining 10, 35, and 60 NCEs into one fragmentation scan, an underfill ratio of 10%, an intensity threshold of 1.3 × 105 counts, and the dynamic exclusion was set to 3 s. Scan range was 200–2000 m/z with a fixed first mass at 50 m/z.

2.10.3. Data processing

Preprocessing of the data (peak detection, integration, peak filtration, peak identification, peak grouping and smoothing, retention time correction, integration, annotation), QC (metabolites correlation analysis) and statistical analysis (univariate testing and multivariate modeling) were conducted on the online and freely available Workflow4Metabolomics (W4M) platform (https://workflow4metabololomics.org), which provided a high-performance and user-friendly environment for computational analysis [32]. Detailed steps and parameters that were used for the different steps are publicly available on the W4M repository (https://workflow4metabolomics.usegalaxy.fr/u/sblat/w/hos-mtaboo-p3-neg-imported-from-uploaded-file and https://workflow4metabolomics.usegalaxy.fr/u/sblat/w/workflow-constructed-from-history-hos-p3-rp-pos-imported-from-uploaded-file for the negative and positive ionization modes respectively).

Principal component analysis (PCA) was used for multivariate exploration of clusters and trends among the observations. Orthogonal supervised partial least-squares-discriminant analysis (OPLS-DA) were also built (the significance of the Q2Y prediction performance metric was assessed by comparison with 1000 models built after random permutation of the response values). The variable that were significant for the classification performances between treatments (OPLS-DA) were selected with Biosigner wrapper

algorithm [33]. A non-supervised analysis was performed using WGCNA (see below) to identify key features.

2.10.3.1. Weighted correlation network analysis (WGCNA). WGCNA [12] was performed using WGCNA R package to identify networks based on correlation analysis, and specifically to identify variables of cecal microbiota, plasma metabolome and brain mRNA expression that were associated with traits of interest (type of surgery and BOLD fMRI responses). WGCNA was performed separately on three datasets (brain mRNA expression, plasma metabolomic profiles and cecal microbiota composition). As final integrative analysis required the same number of animals in each dataset, metabolomic and brain gene analyses for the animal that did permit the microbiota analysis were excluded. Consequently, WGCNA analysis was performed on 7 minipigs in the RYGBP vs. 8 in the SHAM group. For each of these datasets, the correlation matrix identified interconnected features (*e.g.*, genes, metabolite features or OTUs) and assigned them to coexpression modules. One module (the grey one) was reserved for features that did not show enough coexpression metrics. In plasma metabolome and microbiota WGCNA analyses, highly correlated modules were then merged using the Euclidean distance (cut height) depending on visual interpretation of the clustering dendrogram of OTUs or features metabolites. The assigned modules, differentiated by colors, were summarized by eigenvector for each animal (sample). Associations between animals' traits (i.e., type of surgery, BOLD fMRI responses, and gender) and modules were identified with Spearman correlation test (Sup. Figures 1–3 corresponding to WGCNA analysis steps in each sublayer). Modules significantly associated with surgery type or BOLD fMRI responses were used for further analysis. OPLS regressions were performed in selected modules to compute the Variable Importance Projection (VIP) score and the adjusted P-value from Spearman correlation test of each feature with the trait of interest. Features with a VIP score >1 and an adjusted P-value <0.05 were considered as drivers of those modules.

2.10.3.2. Multi-WGCNA analysis strategy. Association between WGCNA modules generated from the 3 datasets were explored using modules eigenvectors correlation. Modules significantly associated together and associated with traits of interest were selected on the basis of Spearman correlations. With those modules of interest, a bipartite network was constructed using two-by-two Spearman correlations and only high |r| coefficient was retained (i.e., $\geq$0.8) for illustration. Modules with no significant association were not depicted.

3.5. Statistical analysis

All analyses were performed using the open-source R statistical software (R: A Language and Environment for Statistical Computing; R Core Team, R Foundation for Statistical Computing, Vienna, Austria; https://www.r-project.org/). Following packages were used: WGCNA, DeSeq2, Phyloseq, ropls, ggplot2. For simple comparisons, we ran nonparametric Mann–Whitney U tests. For repeated comparisons, we ran Type-III ANOVAs to test the Surgery type * Time interaction with post hoc Tukey tests for repeated measures.

4. Results

Zootechnical data were already reported by Gautier and al [18]. Briefly, daily food consumption and weight loss data are illustrated in Fig. 2.

4.1. Analysis of functional MRI brain responses to oral sucrose stimulation after RYGBP compared to diet restriction-induced weight loss (SHAM procedure) (Fig. 3)

4.1.1. Brain responses to sucrose 5%

Brain activation maps (Fig. 3_A). Differences in brain responses to sucrose 5% were detected between the RYGBP and SHAM groups. The brain regions involved in the reward and motivation processes [34], including the caudate nucleus (Cd, higher response in Sham) and the putamen (Put, higher response in RYGBP), exhibited opposite BOLD responses between groups. Brain regions involved in the inhibitory cognitive control and motivation [35] such as the anterior prefrontal cortex (A-PFC) and the dorsal lateral prefrontal cortex (DL-PFC) presented higher brain responses in the RYGBP compared to the SHAM group. Higher brain responses in the RYGBP group were also detected in the prepyriform (PP, an olfactory relay [36]), the insular cortex (IC, a gustatory center [37]) and the amygdala (AMY, associated learning and limbic functions [38]).

Corrected small volume correction (SVC)-based statistics (Fig. 3_B). The SVC analysis confirmed the brain activation maps with contrasted brain responses between groups in reward/motivation brain regions: Higher brain responses in the Cd in the SHAM group and higher bilateral brain responses of Put in the RYGBP group. Higher brain responses in the A-PFC (P_{uncor}=<0.01) and the left DL-PFC (P_{uncor}<0.001, P_{FWE} <0.05) were also detected in the RYGBP group compared to the SHAM group.

4.1.2. Brain responses to sucrose 15%

Brain activation maps *(*Fig. 3_A*).* Compared to control stimulation, sucrose 15% promoted different brain responses between the RYGBP and SHAM groups. The RYGBP group presented higher brain responses in the Cd and the left DL-PFC. In the SHAM group, brain responses were higher in the A-PFC and the right DL-PFC. Higher brain responses were detected in the Put and IC in both groups but in different subdivisions of these structures. Higher brain responses in the SHAM group were identified in the PP area.

Corrected SVC-based statistic *(*Fig. 3_B*).* The SVC analysis confirmed the brain activation maps with a contrasted brain activation in motivation centers: Higher brain responses in the Cd (bilateral, the right Cd reaching FWE corrected significance (P_{uncor} = 0.001, P_{FWE} <0.05) for the RYGBP group and higher brain responses in the Put for the SHAM group (P_{uncor}<0.01). Similar contrasted results were found in the inhibitory cognitive control brain regions: Higher brain responses in the left DL-PFC for the RYGBP group (P_{uncor}<0.01) and higher brain responses in the left A-PFC for the SHAM group (P_{uncor}<0.01).

4.1.3. Effect of a 3-fold increase in sucrose concentration (sucrose 15% vs. sucrose 5%) on brain activations

Brain activation maps *(*Fig. 3_A*).* A 3-fold increased concentration of sucrose stimulation induced different brain responses between RYGBP and SHAM animals. In motivational centers, higher brain responses in the Cd for the RYGBP group and higher brain responses in the Put for the SHAM group were detected. The orbitofrontal cortex (OFC), involved in the hedonic value of the gustatory stimulation [35], presented higher brain responses in the RYGBP group. The PP, considered as an olfactory relay [36], as well as the IC, a gustatory and multisensory integration center [37], presented higher brain responses in the SHAM group, but a different subdivision of the IC presented higher brain responses in the RYGBP group. Higher brain responses in the inhibitory cognitive control centers [35] were finally observed in the A-PFC and the DL-PFC, for both groups but in different subdivisions of these brain regions.

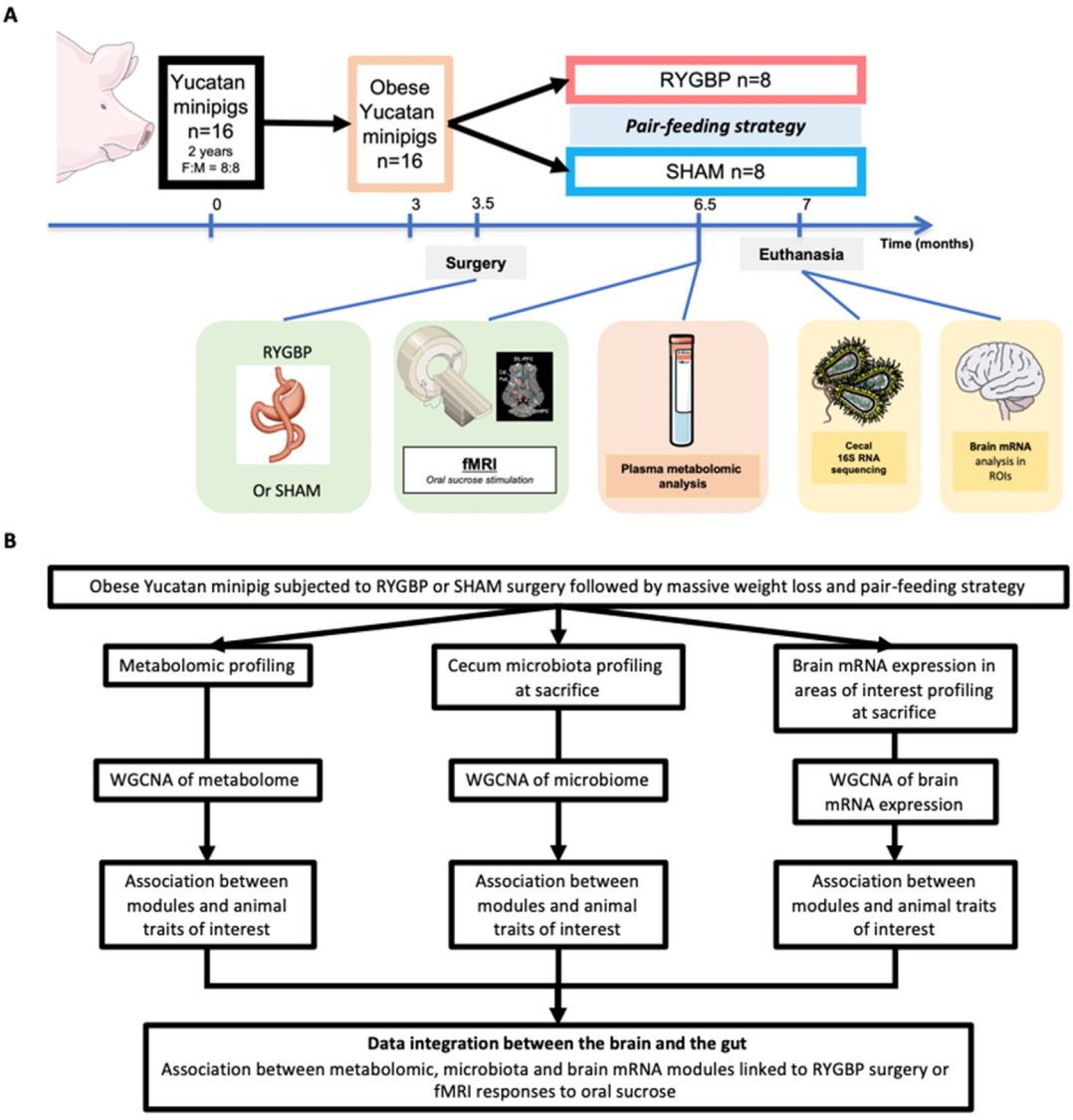

Fig. 1. Study design **(A)** Overview of the study experiment and **(B)** analysis strategy. RYGBP, Roux-en-Y gastric bypass; fMRI, functional magnetic resonance imaging; ROIs, regions of interest planned "a priori"; WGCNA, weighted correlation network analysis; F, female; M, male. Schematic representation used were provided by Servier medical art® (smart.servier.com).

Corrected SVC-based statistic *(*Fig. 3_B*)*. The SVC analysis confirmed the brain responses in motivation centers: Higher brain responses in the Cd (P_{uncor}<0.001, P_{FWE} <0.05) for the RYGBP group, and higher brain responses in the Put for the SHAM group. The A-PFC, involved in impulse control, emotions and decision-making, was modulated in both groups, but in different subdivisions (P_{uncor}<0.01). Interestingly in the RYGBP group, higher brain responses were observed in the OFC (bilateral, P_{uncor}<0.01), a brain structure involved in the gustatory valence and hedonic value of the stimulation.

Specific effects of RYGBP on brain mRNA expression compared to diet restriction-induced weight loss (SHAM procedure). Four months after surgery, mRNA expression in brain ROIs were modified after RYGBP compared to diet restriction-induced weight loss following SHAM procedure. Genes that were significantly up or down regulated between SHAM and RYGBP groups according to brain ROIs are listed in Fig. 4.

Impact of RYGBP on brain anorexigenic and orexigenic gene expression. Among the selected genes involved in appetite regulation (Agouti Related Neuropeptide (AgRP), Neuropeptide Y (NPY), Cocaine and amphetamine regulated transcript protein (CART), Brain derived neurotrophic factor (BDNF), Neuropeptide Y receptor Y2 (NPYY), Glucagon like peptide receptor 1 (GLP1 R) and Proopiomelanocortin (POMc)) and investigated in the four brain ROIs considered. Compared to SHAM, only trends for Leptin receptor (LEPR) mRNA expression in the hypothalamus (up-regulated, P = 0.084), the hippocampus (up-regulated, P = 0.073), and the prefrontal lobe (down-regulated, P = 0.073) were identified in the RYGBP group.

Impact of RYGBP on brain mRNA expression of genes related to inflammation or oxidative stress. Compared to SHAM, mRNA expression of Tumor necrosis factor alpha receptor 1 (TNFα) (in hippocampus P = 0.065 and striatum P = 0.054) and Allograft Inflammatory Factor 1 (AIF1) (in hypothalamus P = 0.074), both of them being involved in inflammation processes, tended to be lower in the RYGBP group.

Impact of RYGBP on brain mRNA expression of genes implicated in the serotoninergic system. Compared to SHAM, the RYGBP

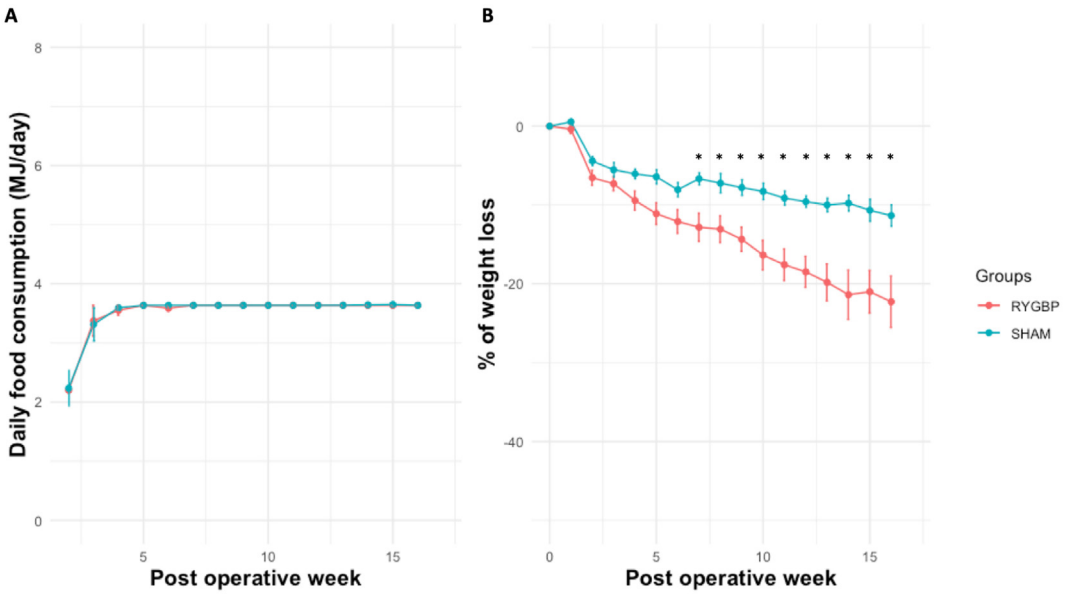

Fig. 2. Animal monitoring (A) Daily food intake (MJ/day) and **(B)** percent of weight loss after surgery according to group allocution. RYGBP, Roux-en-Y gastric bypass. *: Time x Surgery type interaction, P value < 0.001 with Type-III ANOVAs with post hoc Tukey tests for repeated measures.

group exhibited a modification of mRNA expression involved in the serotoninergic system in different brain ROIs. 5-Hydroxytryptamine Receptor 1 A (HTR1a) mRNA expression was higher in the prefrontal lobe (P = 0.036) and the striatum (P = 0.033), whereas mRNA expression of 5-Hydroxytryptamine Receptor 1 F HTR1F was lower in the hypothalamus (P = 0.028) in RYGBP compared to SHAM animals.

Impact of RYGBP on brain gastrointestinal hormones receptor mRNA expression. Compared to SHAM, mRNA expression of insulin receptor (RINS, P = 0.046) and Cannabinoid Receptor 1 (CB1, P = 0.049) of the RYGBP group was significantly upregulated in the hypothalamus. A trend for an increase of Cholecystokinin B Receptor (CCKBR, P = 0.073) was also observed in the hypothalamus.

Impact of RYGBP on mRNA expression implicated in nutrient and short-chain fatty acids transport and blood brain barrier. Compared to SHAM, Monocarboxylate Transporter 1 MCT1 (P = 0.040) mRNA expression was lower in the hypothalamus and Long-chain Fatty Acid Transport Protein 1 SLC27A1 (P = 0.022) mRNA expression was higher in the striatum of the RYGBP group. In the hypothalamus, we observed a trend for decreased marveld2 (P = 0.091), Occludin OCLN (P = 0.086), and increased Platelet-derived growth factor receptor B PDGFRB (P = 0.060) mRNA expression in the RYGBP group.

4.2. Evaluation of fecal fermentation activity and cecal microbiota composition in SHAM and RYGBP groups

From 6 weeks after surgery, RYGBP animals presented significantly higher levels of fecal SCFAs compared to SHAM (P = 0.01, Fig. 5_A) and this difference persisted until sacrifice at 4 months. Cecal α-diversity analysis (Fig. 5_B) showed that RYGBP animals presented a significantly lower bacterial richness compared to SHAM (Observed and Chao1 indices significantly different, P = 0.02 and 0.01 respectively) while Shannon and InvSimpson indices for equitability were not different between groups. Cecal β-diversity explored through Bray Curtis distance and Weight-Unifrac significantly discriminated RYGBP and SHAM groups (permanova, P = 0.001 and 0.002 respectively) (Fig. 5_C).

Among the OTUs revealed with differential abundance analysis, 225 were retained with adjusted P < 0.05. Those corresponded to 10 phyla and 29 families (Sup. Table 3). Firmicutes represented the majority (66%) of the differentially abundant phyla with 9 different families represented. Some phyla, Actinobacteria, Proteobacteria, Fusobacteria and Epsilonbacteria were significantly increased in the RYGBP group (adjusted P < 0.05). Those results are summarized in Fig. 5_D and 5_E.

4.3. Long-term plasma metabolome analysis between SHAM and RYGBP animals (Fig. 6)

Data processing resulted in the detection of 2331 and 2659 ion features in the positive and negative ionization modes, respectively. Multivariate analysis by PCA was used first to visualize groups, trends, and outliers among observations. The first 4 components captured 55% of the total variation in both ionization modes. Clusters were detected and the surgery effect (RYGBP *vs.* SHAM) and the sex (Male *vs.* Female) were well discriminated. As surgery and sex clusters were orthogonal regarding the two main axes of the PCA, supervised multivariate analysis were also performed using orthogonal partial least-square analysis (OPLS-DA, Fig. 6). Using OPLS-DA, RYGBP and SHAM clusters were very well discriminated, Q2Y prediction performance metric *P*-value was significant (*P* = 0.001) for the negative and the positive mode. Furthermore, using a VIP>1 as a threshold for the most discriminating ion features, 397 and 552 features in the positive and negative modes were particularly relevant in the discrimination between RYGBP and SHAM animals. Amongst them, 60 in the positive mode and 128 in the negative mode were significantly different between groups using a univariate analysis (Wilcoxon, FDR testing correction). Unfortunately, annotation of these discriminating ion features was not possible.

4.4. Data integration results

All data integration was detailed in Table 1 concerning association between WGCNA modules and animal traits of interest.

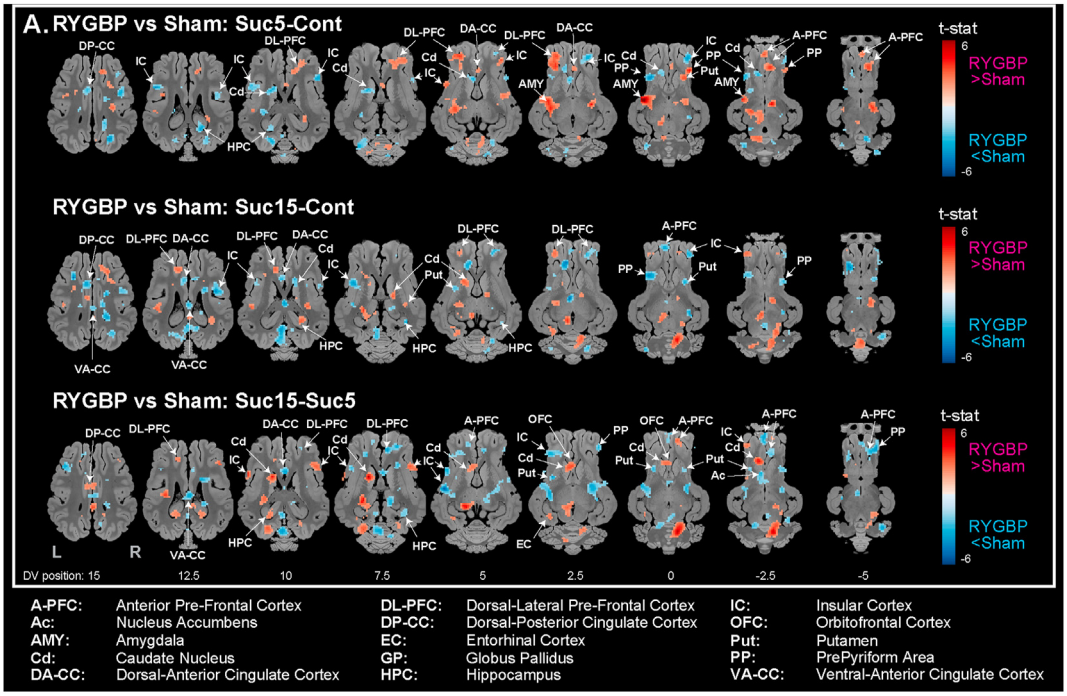

B.

		Suc5-Cont								Suc15-Cont								Suc15-Suc5							
		RYGBP > Sham					RYGBP < Sham			RYGBP > Sham				RYGBP < Sham				RYGBP > Sham				RYGBP < Sham			
ROI	L/R	k	T	p (uncor)	x,y,z		k	T	p (uncor)	x,y,z	k	T	p (uncor)	x,y,z	k	T	p (uncor)	x,y,z	k	T	p (uncor)	x,y,z	k	T	p (uncor)	x,y,z
Ac	R																									
	L																									
Cd	R										31	3.7864	0.0010	-18 12 8 *												
	L						30	3.8718	0.0008	-8 16 9	50	3.2757	0.0028	-7 19 6					71	5.7847	0.0000	-7 17 8 *				
Put	R	21	3.2368	0.0030	9 23 0										20	3.1802	0.0033	9 19 1								
	L	33	3.9051	0.0008	-14 10 3										39	3.3911	0.0022	-10 22 1					20	4.3508	0.0003	-12 17 3
OFC	R																		15	3.2076	0.0032	0 24 2				
	L																		16	3.0893	0.0040	-1 23 2				
A-PFC	R	46	3.3961	0.0022	2 30 -2														57	3.1132	0.0038	-5 38 1	58	3.3758	0.0023	0 41 -2
	L	15	3.1497	0.0035	-1 37 -2										26	3.5682	0.0015	-3 39 1	32	4.7108	0.0002	-3 26 -3	40	3.3022	0.0026	-1 39 -2
DL-PFC	R																									
	L	40	4.0646	0.0006	-10 37 4 *						25	3.5378	0.0016	-10 36 4												

SVC-corrected threshold at p<0.05, ROI number=12
* p-FWE < 0.05

Fig. 3. FMRI brain responses to oral sucrose stimulation after RYGBP compared to diet restriction induced weight loss following sham surgery (A) Brain activation maps to sucrose 5%, sucrose 15% and Effect of a 3-fold increase in sucrose concentration (sucrose-15% vs. sucrose 5%) on brain activations **(B)** Corrected SVC-based statistic in fronto striatal regions implicated in food reward and the inhibitory cognitive control each stimulation. * significant Family Wise Error (FWE) correction at P < 0.05. BP, Roux-en-Y gastric bypass; Suc, Sucrose; Cont, control.

4.4.1. *WGCNA of brain gene expression analysis (detailed in the sup. Figure 1)*

WGCNA clustered the 258 target genes (67 genes in 4 different brain areas, 10 excluded) into 3 modules (Soft power 10, signed type) containing respectively 54, 44 and 74 genes for the 'blue', 'brown', and 'turquoise' modules, respectively. None of them were correlated to RYGBP but 2 modules (the 'blue' and 'brown') were correlated with a fMRI response to sucrose stimulation. Among the 54 genes clustered in the 'blue' module, 5-Hydroxytryptamine (Serotonin) receptor 2 B (5HT2B), Neurotrophin 3 (NTF3), Zonulin 1 (ZO1), Toll-like receptor 4 TLR4 and HTR1F expression in the hippocampus and Interleukin 1 Beta receptor (IL1bR) gene expression in the striatum were identified as drivers (P adjusted<0.05 and VIP score >1) for the correlation with BOLD fMRI responses in the hypothalamus to Sucrose 5% stimulation. The 'brown' module containing 44 genes (mostly from gene expression in the hippocampus, n = 43) was correlated to the Cd and Put BOLD fMRI responses to the oral sucrose 5% stimulation (r = 0.66, P = 0.008) but no gene passed our cut off selection to be defined as driver.

4.4.2. *WGCNA of microbiota analysis (detailed in the sup. Figure 2)*

WGCNA clustered the 848 OTUs into 27 modules (Soft power 14, signed type). The 27 modules correlated were merged into 14 modules using a cut-height of 0.40. Among them, the 'lightcyan' and the 'salmon' modules, containing 52 and 19 OTUs respectively, were highly positively correlated with RYGBP surgery (r = 0.84 P < 0.001 and r = 0.87 P < 0.001 respectively). In those modules, Firmicutes were over-represented. Among the 52 OTUs in the 'lightcyan' module, 9 OTUs (for details please see Fig. 7_A) were identified as drivers (adjusted P < 0.05 and VIP score >1) for the correlation between the module and the RYGBP surgery. Concerning OTUs in the 'salmon' module, none of them reached the conditions to be defined as drivers. Association between the 'midnightblue' module (18 OTUs) and the prefrontal BOLD response to Sucrose 15% stimulation (r = 0.55, P = 0.034) was identified. In this module, 11 OTUs mostly from the Firmicutes phylum (n = 8), were considered as potential drivers (for details please see Fig. 7_A). One module (tan module n = 23) was both correlated with RYGBP and fMRI BOLD responses to Sucrose 15% vs. Sucrose 5% in the hippocampus but no driver was identified for the fMRI BOLD

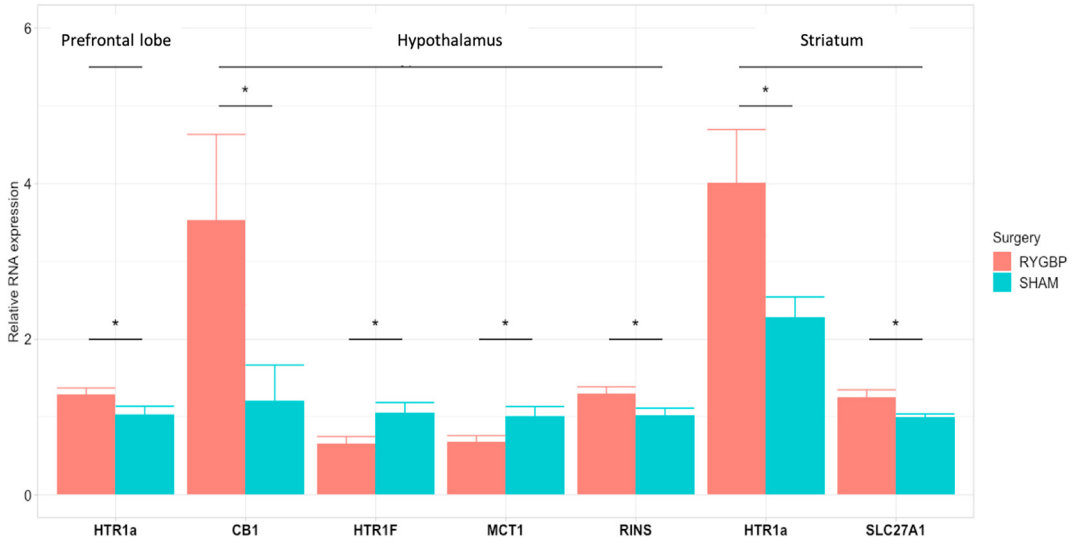

Fig. 4. Brain mRNA expression. Brain gene differentially expressed in brain ROIs between RYGBP and SHAM animals at euthanasia. HTR1a, 5-Hydroxytryptamine Receptor 1 A; CB1, Cannabinoid Receptor 1; HTR1F, 5-Hydroxytryptamine Receptor 1 F; MCT1, Monocarboxylate Transporter 1; RINS, insulin receptor; SLC27A1, Long-chain Fatty Acid Transport Protein 1.

response correlation. However, Lachnospiraceae was identified as a driver for the correlation with the surgery in this module.

4.4.3. *WGCNA of metabolomic analysis (detailed in the sup. Figure 3)*

WGCNA clustered the 4990 metabolites features into 47 modules (Soft power 14, type signed). The 47 modules were merged into 29 modules using a cut-height of 0.25. Among them, the 'magenta' and the 'white' modules, containing 204 and 62 metabolite features respectively, were highly correlated with RYGBP surgery ($r = 0.87$ $P < 0.001$ and $r = 0.87$ $P = 0.0052$ respectively). Other associations between clustered modules and "a priori" selected animal traits are summarized in Table 1, Fig. 7_A and Sup. Figure 3. 111 and 12 metabolites features were identified as potential drivers in the "magenta" and the "white" modules respectively.

4.5. *Data integration (Fig. 7)*

Eigenvectors-based modules identified as highly correlated with RYGBP ('magenta' and 'white' from metabolomics WGCNA or 'lightcyan' and 'salmon' from OTUs WGCNA analysis) were not correlated with brain responses after sucrose stimulation whereas modules based on brain gene expression WGCNA were correlated with brain responses after sucrose stimulation, but not RYGBP. As a consequence, it was not possible to integrate WCGNA-based modules from both OTUS, metabolomics features and brain gene expression with the two animals' traits of interest, type of surgery and brain responses after sucrose stimulation.

However, modules identified as highly correlated with RYGBP in OTUs ('salmon' and 'lightcyan' modules) and metabolomics ('white' and 'magenta' modules) were also correlated with each other based on their eigenvectors (Fig. 7_A). Those subnetworks were used to construct the bipartite network (Fig. 7_B) between OTUs ('lightcyan' and 'salmon' modules) and metabolites features ('white' and 'magenta' modules) from modules of interest (network constructed based on a threshold correlation Spearman $|r| \geq 0.8$). Some OTUs (mostly Firmicutes) appeared to play a central role or 'Hub' regarding the number of connections with different metabolite features.

5. Discussion

This study is the first of its kind to provide a systemic overview of the microbiota–gut–brain axis modifications induced by a Roux-en-Y gastric bypass (RYGBP) in the obese minipig model. Combining brain functional imaging with brain mRNA expression, exploration of the gut microbiota composition/activity and plasma metabololomics, we managed to describe specific effects of RYGBP compared to SHAM surgery with pair-feeding treatment. We showed that RYGBP and SHAM modulated differently the frontostriatal responses to oral sucrose stimulation, suggesting a different hedonic treatment and inhibitory control related to palatable food after surgery. The WGCNA integration analysis also revealed interactions between specific OTUs, plasmatic metabolite features and brain gene expression associated with RYGBP and/or fMRI brain responses to oral sucrose.

5.1. *Brain functional changes*

Obesity-induced specific brain anomalies (*e.g.* lower prefrontal cortex metabolism) have already been documented in minipigs [15] and are similar to those described in obese humans [39]. Only three studies reported fMRI brain responses to food reward receipt after RYGBP in humans [40–42]. Wang et al. (2016) studied reward receipt to sweet *vs.* salty gustatory stimulation [40], while Smith et al. (2020) studied ventral tegmental area (VTA) BOLD signal in response to gustatory stimulation with cream ± 20% sugar [41]. Ten Kulve et al. [42] showed that after RYGBP, GLP-1 receptor blockade resulted in a larger increase in activation of the insula in response to chocolate milk (*i.e.* palatable food) consumption. Though, none of these authors studied an increased concentration of sugar to explore the relationship between sweet intensity and hedonism after RYGBP. Patients with significant weight loss after RYGBP showed higher activity in the DL-PFC during food craving resisting tasks with the presentation of high-energy food pictures [43]. Other studies [44–46] have found an impact of RYGBP on prefrontal cortex (PFC) responses when studying reward anticipation with food pictures or olfactory/auditory stimulations. Here we showed higher BOLD responses to sucrose 5% and 15% in the left DL-PFC of RYGBP compared to SHAM animals, suggesting a better inhibitory

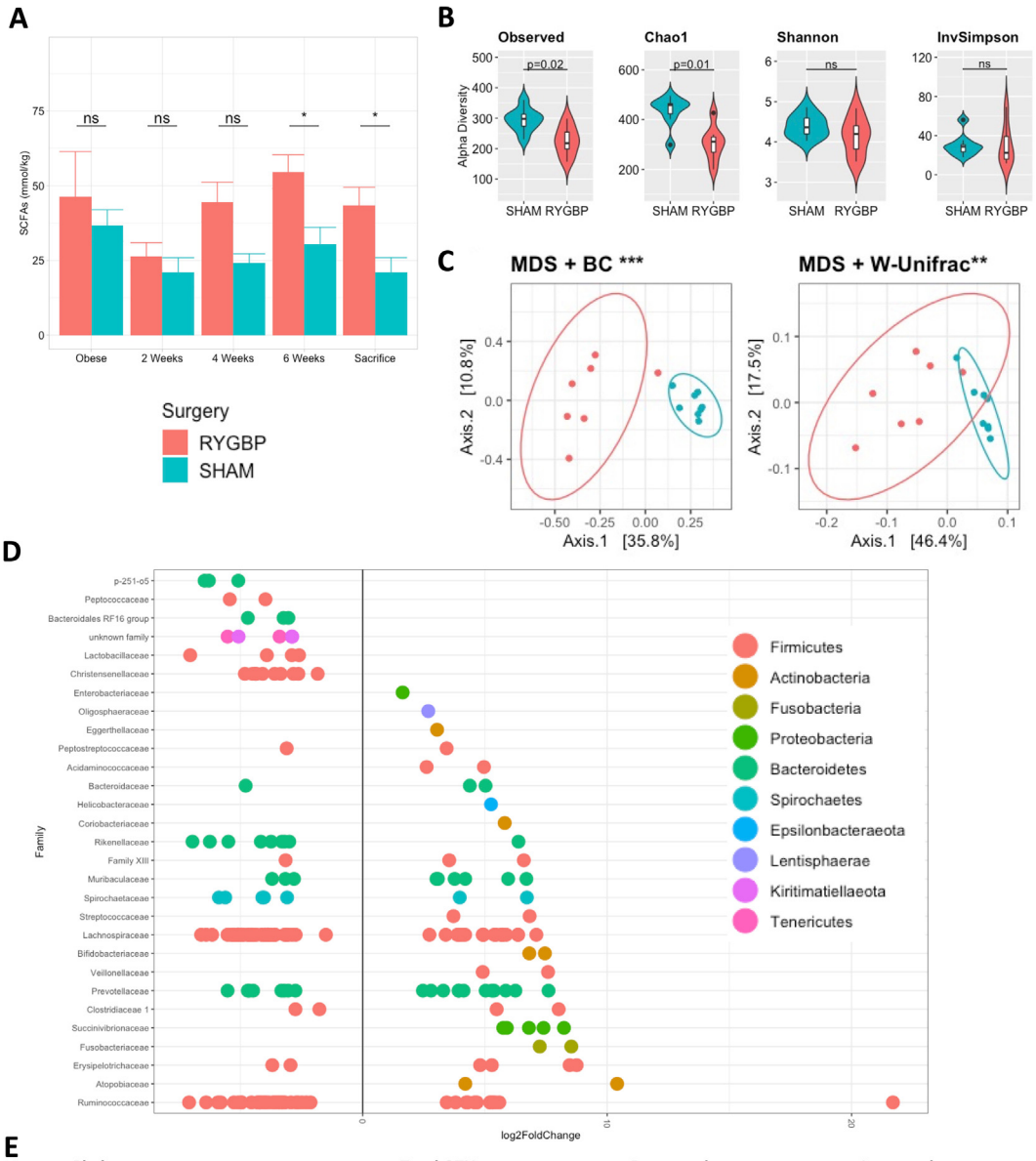

E

Phylum	Total OTUs n=225 (%)		Decreased n=140 (%)		Increased n=85 (%)	
Firmicutes	150	(66.67%)	104	(74.29%)	46	(54.12%)
Actinobacteria	6	(2.67%)	0	(0.00%)	6	(7.06%)
Fusobacteria	2	(0.89%)	0	(0.00%)	2	(2.35%)
Proteobacteria	6	(2.67%)	0	(0.00%)	6	(7.06%)
Bacteroidetes	47	(20.89%)	26	(18.57%)	21	(24.71%)
Spirochaetes	7	(3.11%)	5	(3.57%)	2	(2.35%)
Epsilonbacteraeota	1	(0.44%)	0	(0.00%)	1	(1.18%)
Lentisphaerae	1	(0.44%)	0	(0.00%)	1	(1.18%)
Kiritimatiellaeota	3	(1.33%)	3	(2.14%)	0	(0.00%)
Tenericutes	2	(0.89%)	2	(1.43%)	0	(0.00%)

Repartition at phylum of OTUs revealed with differential abundance analysis (RYGBP vs SHAM) with P value corrected <0.05

Fig. 5. Evaluation of fecal fermentation activity and cecal microbiota composition in SHAM and RYGBP groups (A) Fecal SCFAs level; ns, not significant; * Time x Surgery type interaction, P value < 0.05 with Type-III ANOVAs with post hoc Tukey tests for repeated measures (B) Cecal α-diversity analysis (C) Cecal β-diversity (D) and (E) Differential abundance analysis between RYGBP and SHAM.

control. The A-PFC was also significantly more activated by sucrose 5% in RYGBP animals. In a study aimed at blocking GLP1 receptor before and after obesity surgery, van Duinkerken et al. [47] demonstrated that resting-state functional connectivity changes in the frontoparietal network were related to weight loss and appetite control, and that GLP1 probably had a role in these changes after RYGBP. Another study reported increased postprandial GLP1 concentrations after surgery, which was correlated with brain activity

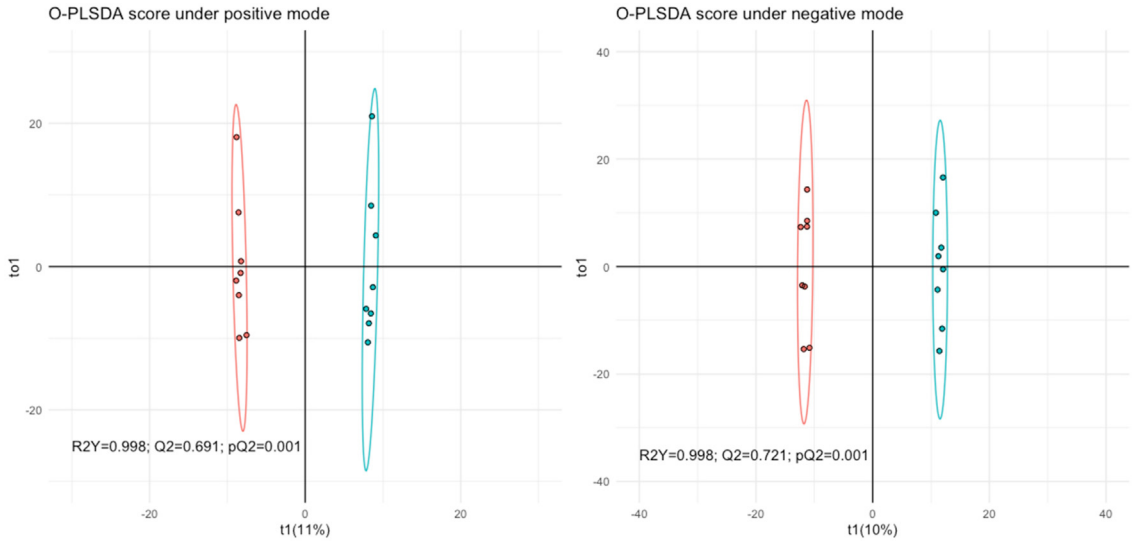

Fig. 6. Plasma metabolomic analysis O-PLSDA score graphs under positive and negative modes.

Table 1
Synthesis of WGCNA module correlations with traits of interest.

Type of analysis	Module color	Features	"A priori" selected animals traits analyzed	Correlation		P value
OTUs n = 848						
Microbiota Analysis[a]	**salmon**	19 (2.24%)	RYGBP	↑	0.87	<0.0001
	lightcyan	52 (6.13%)	RYGBP	↑	0.80	0.0003
	turquoise	187 (22.05%)	RYGBP	↓	−0.87	<0.0001
	red	45 (5.31%)	RYGBP	↓	−0.62	0.014
	cyan	55 (6.49%)	RYGBP	↓	−0.87	<0.0001
	purple	88 (10.38%)	RYGBP	↓	−0.87	<0.0001
	green	48 (5.66%)	RYGBP	↓	−0.87	<0.0001
	black	40 (4.72%)	RYGBP	↓	−0.80	0.0003
	tan	23 (2.71%)	RYGBP	↓	−0.87	<0.0001
			HPC BOLD signal Suc15% vs Suc5%	↓	−0.52	0.046
	midnightblue	18 (2.12%)	Frontal BOLD signal Suc 15% vs Control	↑	0.55	0.034
Genes n = 258						
mRNA brain gene expression[a]	**blue**	54 (20.93%)	HYP BOLD signal Suc 5% vs control	↑	0.54	0.0396
	brown	44 (17.05%)	Cd; Put BOLD signal Suc 5% vs control	↑	0.66	0.0078
Features n = 4990						
Metabolomic[a]	**Magenta**	204 (4.09%)	RYGBP surgery	↑	0.87	<0.0001
	White	62 (1.24%)	RYGBP surgery	↑	0.87	0.0052
	greenyellow	326 (6.53%)	Gender	↑	0.87	<0.0001
			HPC BOLD signal Suc 15% vs control	↓	−0.65	0.009
	sienna3	52 (1.04%)	Cd; Put BOLD signal Suc 5% vs control	↓	−0.68	0.0058
			HPC BOLD signal Suc15% vs Suc5%	↑	0.65	0.0082
	Darkred	168 (3.37%)	Gender	↑	0.65	0.0088
			HPC BOLD signal Suc 5% vs control	↓	−0.55	0.0337
			Hyp BOLD signal Suc 15% vs Suc 5%	↓	−0.61	0.0156
			Hyp BOLD signal Suc 15% vs control	↓	−0.53	0.0400
	Brown	204 (4.09%)	HYP BOLD signal Suc 15% vs Suc 5%	↓	−0.62	0.0134
			RYGBP	↑	0.53	0.0400
	Royalblue	265 (5.31%)	HYP BOLD signal Suc 15% vs Suc 5%	↑	0.60	0.0189
	lightsteelblue1	40 (0.80%)	Frontal BOLD signal Suc 15% vs Suc 5%	↑	0.53	0.0445
	floralwhite	37 (0.74%)	Frontal BOLD signal Suc 15% vs Suc 5%	↑	0.63	0.0127
			Frontal BOLD signal Suc 5% vs control	↓	−0.59	0.0198
	turquoise	301 (6.03%)	HPC BOLD signal Suc15% vs Suc5%	↑	0.54	0.0365
			HPC BOLD signal Suc 5% vs control	↓	−0.53	0.0445
	darkmagenta	800 (16.03%)	HPC BOLD signal Suc 15% vs control	↓	−0.55	0.0337
	Green	247 (4.95%)	HPC BOLD signal Suc 5% vs control	↑	0.59	0.0198
			HPC BOLD signal Suc 15% vs control	↑	0.53	0.04
	black	292 (5.85%)	HPC BOLD signal Suc 5% vs control	↓	−0.62	0.01

[a] Microbiota, above 14 modules, mRNA brain above 4 modules, Metabolomic above 29 modules. RYGBP: Roux and Y gastric bypass; HPC: hippocampus; Cd: caudate nucleus; Put: Putamen; Suc: sucrose; HYP: Hypothalamus; BOLD: Blood Oxygenation Level Dependent.

changes in areas involved in sensory integration, high-level executive functions and decision-related processes [44]. Even though we did not specifically investigate GLP1 in this study, we previously demonstrated that GLP1 plasma levels were increased in our RYGBP obese minipig model compared to SHAM during an oral glucose tolerance test [17].

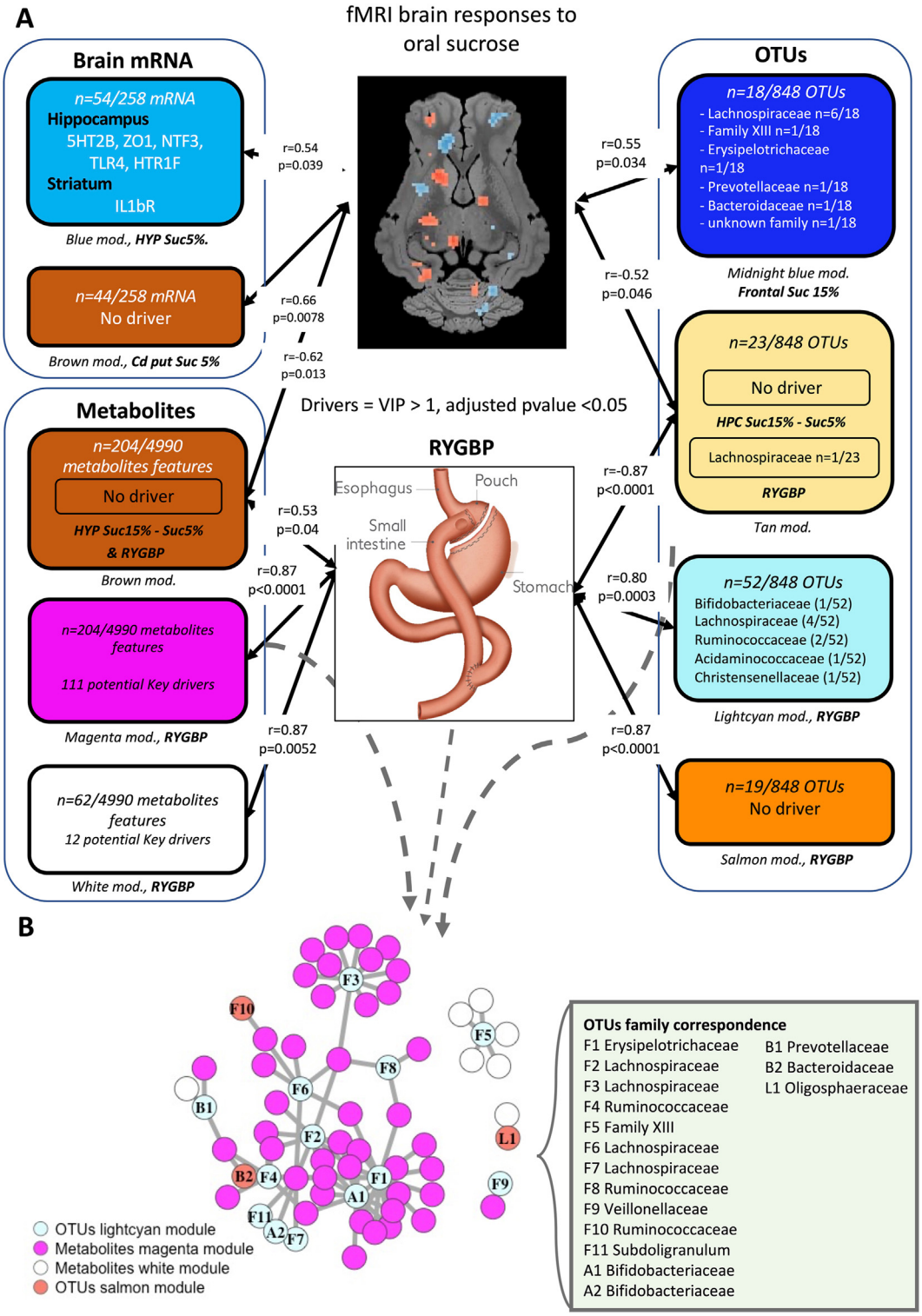

Fig. 7. Integrative analysis synthesis (A) Synthesis of drivers identified in WGCNA modules of interest in brain mRNA expression WGCNA, cecum microbiota WGCNA and metabolomic WGCNA. Drivers were identified in modules correlated with traits of interest such as fMRI BOLD responses to sucrose stimulation or RYGBP surgery. Features with a VIP score >1 and an adjusted P-value <0.05 were considered as drivers of those modules **(B)** Bipartite network between OTUs ('lightcyan' and 'salmon' modules) and metabolites features ('white' and 'magenta' modules) from modules of interest (Spearman Correlation $|r| \geq 0.8$). F, Firmicutes; A, Actinobacteria; B Bacteroides; L, Lentisphaerae.

Significantly higher brain responses in the amygdala (AMY) were observed with sucrose 5% in RYGBP compared to SHAM. AMY is known to receive direct afferences from lingual nerves and to be involved in stimulus pleasantness [48,49]. Using 18 F-FDG PET imaging, we previously reported that RYGBP enhanced brain responses in the striatum and mesolimbic network in response to oral sucrose 16%. We notably showed higher brain metabolism in the dorsal striatum and dorsal posterior cingulate cortex (DP-CC)

compared to SHAM [18]. Similarly, in the present study sucrose stimulation led to increased activity in the dorsal striatum. The Cd was especially increased in RYGBP compared to SHAM for the contrast sucrose 15% *vs*. 5%, demonstrating that RYGBP potentiated the Cd response to high-sweet taste. In addition to reward, Cd is also known to be involved in the inhibitory cognitive control [50] and working memory in conjunction with the hippocampus and AMY. Interestingly, sub-regionally changes of striatal dopamine transporter in the dorsal striatum engaged in the hedonic rating of sucrose in humans was recently highlighted, especially in the Cd [51]. After surgery, the orbitofrontal cortex (OFC), involved in the hedonic value of the gustatory stimulation, also presented higher brain responses in the RYGBP group when the sucrose concentration was 3-fold increased. Altogether, these brain functional changes support the hypothesis of an increased reward perception and inhibitory control after RYGBP, which is also supported by previous data published in the same animals, highlighting more attention and less anxiety after weight loss during a food-rewarded cognitive test, as well as less food ingested in RYGBP compared to SHAM during a two-choice feeding test [18].

5.2. Brain mRNA expression

In mice, the expression of key genes involved in body weight regulation, appetite and inflammation was studied in the medio basal hypothalamus (HYP) 2 and 12 weeks after RYGBP [52]. Compared to a weight-matched calorie-restricted control group, the significant decreased of AgRP and NPY expression observed at 2 weeks disappeared at 12 weeks. Even though we did not find similar effects on AgRP and NPY mRNA expression, we demonstrated in our minipig model, 4 months after surgery, a significant RYGPB-induced modulation of genes involved in the serotoninergic system such as HTR1a (upregulated in the frontal lobe and the striatum) and HTR1f (down regulated in the HYP), as well as of genes coding for cannabinoid and insulin receptors (upregulated in HYP) and monocarboxylate transporter (downregulated in HYP). The integrative analysis identified two modules (blue and brown) correlated with the BOLD responses to sucrose 5% in the HYP and dorsal striatum, respectively, but with no link with RYGBP. In light of the magnitude of changes (*e.g.* brain mRNA expression [52] or increased GLP1 secretion [17]) observed during the first 15 days after surgery, it would be interesting to perform a new integrative study much earlier than 4 months after surgery to capture the adaptive phase to RYGBP before the onset of a potential equilibrium. The receptors and transporters of which mRNA expressions were modulated by RYGBP all have a role in appetite and food intake control, but the interpretation of these results is tricky because the regions considered (striatum, prefrontal lobe, HYP) were very large and heterogenous. For example, hypothalamic CB1 can have different roles in food intake control [53], depending on the anatomical localization of the receptor, the feeding status and interaction with other hormones such as leptin [54].

5.3. Microbiota and metabolomics

The microbiota composition was specifically impacted by RYGBP as illustrated by the WGCNA analyses. Interestingly, an increased weight loss was observed in RYGBP animals despite similar food intake in both groups due to the pair-feeding strategy in SHAM animals. This suggests either an increased energy expenditure in the RYGBP group or a different metabolic use of nutrients by the host and/or gut microbiota. Such a relationship has already been demonstrated by Tremaroli et al. (2015), using gut microbiota transfer from RYGBP patients to germ-free mice [55]. Indeed, gut microbiota can modify the host energy balance [56] and some microbial metabolites can play a role in the host metabolism and associated disorders, as highlighted in a recent review [57].

Alpha diversity analysis showed that our RYGBP animals presented a significantly lower bacterial richness compared to SHAM. The cecal Firmicutes/Bacteroidetes (F/B) ratio was lower compared to SHAM, which was mostly driven by the increased abundance of Bacteroidetes (data not shown). A previous study in the Ossabaw minipig identified no relationship between the cecal F/B ratio and the % of body fat, contrary to the F/B ratio in fecal microbiota [58]. In the WGCNA lightcyan module generated, we identified Bifidobacterium as a key driver highly associated with RYGBP. Interestingly, Bifidobacterium was also found increased in humans after RYGBP [59]. The differential weight loss between the two groups might be attributed to an increased microbial fermentation activity of polysaccharides into SCFAs, as already described in mice who received gut microbiota from RYGBP mice [60]. SCFAs-producing bacteria such as Blautia [61] were found increased in RYGBP. SCFAs are known to be involved in the host lipogenesis and gluconeogenesis, and butyrate for example was found to improve insulin sensitivity and increase energy expenditure in mice [62]. All the Proteobacteria that increased after RYGBP were linked to Gammaproteobacteria, previously identified as the most consistent class impacted by bariatric surgery [6] and likely related with metabolic improvement. Zizmare et al. [63] observed similar results in terms of weight loss in a rat obesity model between pair-fed SHAM and RYGBP after surgery but our results on the concentration of SCFAs in the stool were the opposite (*i.e.* higher in the RYGBP group in our study). Comparison of microbiota profiles between this study and ours is not possible because we only analyzed the cecal microbiota. Plasma metabolomics analyses showed that two modules were highly correlated with RYGBP while many others were associated only with brain responses to oral sucrose. The overall integration analysis, combining WGCNA on OTUs and metabolomic features, identified a few metabolites of interest associated with the Firmicutes phylum and more expressed after RYGBP, but the annotation and identification of metabolites is a tricky process that would need further confirmation with complementary analytic methods.

5.4. Limitations

Even though the number of animals was quite low for the fMRI analyses, the alpha risk was controlled with adequate statistical analysis, corrected *P*-values and a limited number of a priori ROIs. More ROIs may have provided interesting insight but at the cost of a decreased statistical power. Addition of obese and normal-weight control groups might have been valuable but the overall project was already long, costly and highly complex in terms of logistic. To date, we found no other equivalent of such a longitudinal preclinical study in a large animal model. Despite identification of significant changes of the plasma metabolome with RYGBP, we were not able to provide strong annotation of key driver metabolites. A precise and comprehensive annotation would require a fully dedicated project with much potent analytical methods. Even though WGCNA analyses have to be interpreted cautiously because no causal relationship can be derived, our work illustrates the possibility to explore systemic modulations/disruptions of the microbiota–gut–brain axis.

6. Conclusion

This longitudinal study illustrates the mid-term consequences of RYGBP in obese Yucatan minipigs compared to animals subjected to a SHAM surgery and pair-feeding procedure. We have successively demonstrated the profound modifications induced by RYGBP

in functional brain responses to oral sucrose stimulation related to food reward, hedonic evaluation and inhibitory control. RYGBP modified the expression of mRNA of brain genes involved in the serotoninergic and cannabinoid systems, but also nutrient and SCFAs transport. Even with a pair-feeding strategy in the control group, the cecal microbiota was deeply modified by the RYGBP, which likely illustrates the role of microbiota metabolites as also suggested by the WGCNA integrative analysis. In the light of all of these data, our model represents a great opportunity to improve, through integrative and systemic analyses, our knowledge about the complex neurocognitive and metabolic changes induced by RYGBP, even though further studies are necessary to explore the early-onset dynamic of these adaptations.

Data availability

The dataset for this study can be found in the INRAE open-access repository: https://doi.org/10.57745/EFUZ2E.

Ethical approval

This protocol was approved by the local Ethics Committee CREEA (Rennes Committee of Ethics in Animal Experimentation) (authorization #201504280924565) and the Ministry of Higher Education and Research (Reference No APAFIS #598–201 504 280 924 565 v5).

Compliance with ethical standards

The experiments presented in this paper were conducted at the INRA center of St Gilles (Agreement No 3527532), France, in accordance with the current ethical standards of the European Community (Directive 2010/63/EU).

Financial support

This study was funded by the Hed-O-Shift INRA Priority Action of the AlimH Division (Nutrition, Chemical Food Safety and Consumer Behaviour) and coordinated by David Val-Laillet. Damien Bergeat also received funding from the European Society for Clinical Nutrition and Metabolism to perform part of this project.

Author contributions

Damien Bergeat: Conceptualization; Formal analysis; Funding acquisition; Investigation; Methodology; Validation; Visualization; Roles/Writing – original draft; Writing – review & editing. **Nicolas Coquery**: Conceptualization; Data curation; Formal analysis; Investigation; Methodology; Writing – review & editing. **Yentl Gautier**: Formal analysis; Investigation; MethoWriting – review & editing. **Sarah Clotaire**: Formal analysis; Writing – review & editing. **Émilie Vincent**: Formal analysis; Writing – review & editing. **Véronique Romé**: Formal analysis; Writing – review & editing. **Sylvie Guérin**: Investigation; Methodology; Writing – review & editing. **Isabelle Le Huërou-Luron**: Formal analysis; Methodology; Resources; Supervision; Validation; Writing – review & editing. **Sophie Blat**: Formal analysis; Methodology; Resources; Supervision; Validation; Writing – review & editing. **Ronan Thibault**: Conceptualization; Funding acquisition; Supervision; Validation; Writing – review & editing. **David Val-Laillet**: Conceptualization; Funding acquisition; Investigation; Methodology; Project administration; Supervision; Validation; Visualization; Roles/Writing – original draft; Writing – review & editing.

Conflicts of interest

The authors declare no competing interest.

All authors have completed the ICMJE uniform disclosure form at http://www.icmje.org/coi_disclosure.pdf (available on request from the corresponding author) and declare that (1) No authors have support from any company for the submitted work; (2) None has relationships (travel/accommodations expenses covered/reimbursed) who might have an interest in the work submitted in the previous three years. None have no relationship with any company that might have an interest in the work submitted; (3) no author's spouse, partner, or children have any financial relationships that could be relevant to the submitted work; and (4) none of the authors has any non-financial interests that could be relevant to the submitted work.

Acknowledgements

We acknowledge the entire EAT team for their technical support at different steps of the study, especially Régis Janvier and Isabelle Nogret. The authors want to thank all the staff from the Rennes pig experimental facilities (UE3P): Alain Chauvin, Julien Georges, Mickaël Génissel, Francis Le Gouevec, Bruno Fontaine and Renan Delaunay for their technical support. We acknowledge the PRISM (Plateforme de Recherche en Imagerie et Spectroscopie Multimodales, Rennes, France) core facility for its technical support, and especially Stéphane Quellec. We thank the Biogenouest-Corsaire core facility that supported this work, in particular Sadia Ouzia and Lauriane Rambaud from the MELISA platform for all the LC-HRMS analysis.

Appendix A. Supplementary data

Supplementary data to this article can be found online at https://doi.org/10.1016/j.clnu.2023.01.015.

References

[1] Carlsson LMS, Sjöholm K, Jacobson P, Andersson-Assarsson JC, Svensson P-A, Taube M, et al. Life expectancy after bariatric surgery in the Swedish obese subjects study. N Engl J Med 2020;383:1535–43. https://doi.org/10.1056/NEJMoa2002449.

[2] Mingrone G, Panunzi S, De Gaetano A, Guidone C, Iaconelli A, Capristo E, et al. Metabolic surgery versus conventional medical therapy in patients with type 2 diabetes: 10-year follow-up of an open-label, single-centre, randomised controlled trial. Lancet 2021;397:293–304. https://doi.org/10.1016/S0140-6736(20)32649-0.

[3] Sinclair P, Brennan DJ, le Roux CW. Gut adaptation after metabolic surgery and its influences on the brain, liver and cancer. Nat Rev Gastroenterol Hepatol 2018;15:606–24. https://doi.org/10.1038/s41575-018-0057-y.

[4] Liu R, Hong J, Xu X, Feng Q, Zhang D, Gu Y, et al. Gut microbiome and serum metabolome alterations in obesity and after weight-loss intervention. Nat Med 2017;23:859–68. https://doi.org/10.1038/nm.4358.

[5] Aron-Wisnewsky J, Prifti E, Belda E, Ichou F, Kayser BD, Dao MC, et al. Major microbiota dysbiosis in severe obesity: fate after bariatric surgery. Gut 2019;68:70–82. https://doi.org/10.1136/gutjnl-2018-316103.

[6] Debédat J, Clément K, Aron-Wisnewsky J. Gut microbiota dysbiosis in human obesity: impact of bariatric surgery. Curr Obes Rep 2019;8:229–42. https://doi.org/10.1007/s13679-019-00351-3.

[7] Torres-Fuentes C, Schellekens H, Dinan TG, Cryan JF. The microbiota–gut–-brain axis in obesity. Lancet Gastroenterol Hepatol 2017;2:747–56. https://doi.org/10.1016/S2468-1253(17)30147-4.

[8] Karlsson HK, Tuominen L, Helin S, Salminen P, Nuutila P, Nummenmaa L. Mesolimbic opioid-dopamine interaction is disrupted in obesity but recovered by weight loss following bariatric surgery. Transl Psychiatry 2021;11:259. https://doi.org/10.1038/s41398-021-01370-2.

[9] Scholtz S, Miras AD, Chhina N, Prechtl CG, Sleeth ML, Daud NM, et al. Obese patients after gastric bypass surgery have lower brain-hedonic responses to food than after gastric banding. Gut 2014;63:891–902. https://doi.org/10.1136/gutjnl-2013-305008.

[10] Scholtz S, Miras AD, Chhina N, Prechtl CG, Sleeth ML, Daud NM, et al. Obese patients after gastric bypass surgery have lower brain-hedonic responses to

food than after gastric banding. Gut 2014;63:891–902. https://doi.org/10.1136/gutjnl-2013-305008.
[11] Ochner CN, Kwok Y, Conceição E, Pantazatos SP, Puma LM, Carnell S, et al. Selective reduction in neural responses to high calorie foods following gastric bypass surgery. Ann Surg 2011;253:502–7. https://doi.org/10.1097/SLA.0b013e318203a289.
[12] Langfelder P, Horvath S. WGCNA: an R package for weighted correlation network analysis. BMC Bioinf 2008;9:559. https://doi.org/10.1186/1471-2105-9-559.
[13] Guilloteau P, Zabielski R, Hammon HM, Metges CC. Nutritional programming of gastrointestinal tract development. Is the pig a good model for man? Nutr Res Rev 2010;23:4–22. https://doi.org/10.1017/S0954422410000077.
[14] Roura E, Koopmans S-J, Lallès J-P, Le Huerou-Luron I, de Jager N, Schuurman T, et al. Critical review evaluating the pig as a model for human nutritional physiology. Nutr Res Rev 2016;29:60–90. https://doi.org/10.1017/S0954422416000020.
[15] Val-Laillet D, Layec S, Guérin S, Meurice P, Malbert C-H. Changes in brain activity after a diet-induced obesity. Obesity 2011;19:749–56. https://doi.org/10.1038/oby.2010.292.
[16] Baud G, Daoudi M, Hubert T, Raverdy V, Pigeyre M, Hervieux E, et al. Bile diversion in roux-en-Y gastric bypass modulates sodium-dependent glucose intestinal uptake. Cell Metabol 2016;23:547–53. https://doi.org/10.1016/j.cmet.2016.01.018.
[17] Bergeat D, Blat S, Gautier Y, Guérin S, Le Huërou-Luron I, Thibault R, et al. A pilot study about the development and characterization of a Roux en Y gastric bypass model in obese Yucatan minipigs. Sci Rep 2021;11:20190. https://doi.org/10.1038/s41598-021-98575-8.
[18] Gautier Y, Bergeat D, Serrand Y, Réthoré N, Mahérault M, Malbert C-H, et al. Western diet, obesity and bariatric surgery sequentially modulated anxiety, eating patterns and brain responses to sucrose in adult Yucatan minipigs. Sci Rep 2020;10:20130. https://doi.org/10.1038/s41598-020-76910-9.
[19] Coquery N, Meurice P, Janvier R, Bobillier E, Quellec S, Fu M, et al. fMRI-based brain responses to quinine and sucrose gustatory stimulation for nutrition research in the minipig model: a proof-of-concept study. Front Behav Neurosci 2018;12:151. https://doi.org/10.3389/fnbeh.2018.00151.
[20] Coquery N, Adam J-F, Nemoz C, Janvier R, Livingstone J, Chauvin A, et al. Locomotion and eating behavior changes in Yucatan minipigs after unilateral radio-induced ablation of the caudate nucleus. Sci Rep 2019;9:1–11. https://doi.org/10.1038/s41598-019-53518-2.
[21] Coquery N, Menneson S, Meurice P, Janvier R, Etienne P, Noirot V, et al. fMRI-based brain responses to olfactory stimulation with two putatively orexigenic functional food ingredients at two different concentrations in the pig model. J Food Sci 2019;84:2666–73. https://doi.org/10.1111/1750-3841.14772.
[22] Menneson S, Serrand Y, Janvier R, Noirot V, Etienne P, Coquery N, et al. Regular exposure to a Citrus-based sensory functional food ingredient alleviates the BOLD brain responses to acute pharmacological stress in a pig model of psychosocial chronic stress. PLoS One 2020;15:e0243893. https://doi.org/10.1371/journal.pone.0243893.
[23] Clouard C, Jouhanneau M, Meunier-Salaün M-C, Malbert C-H, Val-Laillet D. Exposures to conditioned flavours with different hedonic values induce contrasted behavioural and brain responses in pigs. PLoS One 2012;7:e37968. https://doi.org/10.1371/journal.pone.0037968.
[24] Hellekant G, Danilova V, Ninomiya Y. Primate sense of taste: behavioral and single chorda tympani and glossopharyngeal nerve fiber recordings in the rhesus monkey, Macaca mulatta. J Neurophysiol 1997;77:978–93. https://doi.org/10.1152/jn.1997.77.2.978.
[25] Vandesompele J, De Preter K, Pattyn F, Poppe B, Van Roy N, De Paepe A, et al. Accurate normalization of real-time quantitative RT-PCR data by geometric averaging of multiple internal control genes. Genome Biol 2002;3. https://doi.org/10.1186/gb-2002-3-7-research0034. RESEARCH0034.
[26] Lemaire M, Dou S, Cahu A, Formal M, Normand LL, Romé V, et al. Addition of dairy lipids and probiotic Lactobacillus fermentum in infant formula programs gut microbiota and entero-insular axis in adult minipigs. Sci Rep 2018;8. https://doi.org/10.1038/s41598-018-29971-w.
[27] Anahtar MN, Bowman BA, Kwon DS. Efficient nucleic acid extraction and 16S rRNA gene sequencing for bacterial community characterization. J Vis Exp JoVE 2016. https://doi.org/10.3791/53939.
[28] Mahé F, Rognes T, Quince C, de Vargas C, Dunthorn M. Swarm v2: highly-scalable and high-resolution amplicon clustering. PeerJ 2015;3:e1420. https://doi.org/10.7717/peerj.1420.
[29] Chen L, Reeve J, Zhang L, Huang S, Wang X, Chen J. GMPR: a robust normalization method for zero-inflated count data with application to microbiome sequencing data. PeerJ 2018;6:e4600. https://doi.org/10.7717/peerj.4600.
[30] Love MI, Huber W, Anders S. Moderated estimation of fold change and dispersion for RNA-seq data with DESeq2. Genome Biol 2014;15:550. https://doi.org/10.1186/s13059-014-0550-8.
[31] Bligh EG, Dyer WJ. A rapid method of total lipid extraction and purification. Can J Biochem Physiol 1959;37:911–7. https://doi.org/10.1139/o59-099.
[32] Giacomoni F, Le Corguille G, Monsoor M, Landi M, Pericard P, Petera M, et al. Workflow4Metabolomics: a collaborative research infrastructure for computational metabolomics. Bioinformatics 2015;31:1493–5. https://doi.org/10.1093/bioinformatics/btu813.
[33] Rinaudo P, Boudah S, Junot C, Thévenot EA. Biosigner: a new method for the discovery of significant molecular signatures from omics data. Front Mol Biosci 2016;3. https://doi.org/10.3389/fmolb.2016.00026.
[34] Haber SN. Corticostriatal circuitry. Dialogues Clin Neurosci 2016;18:7–21. https://doi.org/10.31887/DCNS.2016.18.1/shaber.
[35] Grabenhorst F, Rolls ET. Value, pleasure and choice in the ventral prefrontal cortex. Trends Cognit Sci 2011;15:56–67. https://doi.org/10.1016/j.tics.2010.12.004.
[36] Courtiol E, Wilson DA. The olfactory mosaic: bringing an olfactory network together for odor perception. Perception 2017;46:320–32. https://doi.org/10.1177/0301006616663216.
[37] Staszko SM, Boughter JD, Fletcher ML. Taste coding strategies in insular cortex. Exp Biol Med Maywood NJ 2020;245:448–55. https://doi.org/10.1177/1535370220909096.
[38] McDonald AJ, Mott DD. Functional neuroanatomy of amygdalohippocampal interconnections and their role in learning and memory. J Neurosci Res 2017;95:797–820. https://doi.org/10.1002/jnr.23709.
[39] Le DSNT, Pannacciulli N, Chen K, Del Parigi A, Salbe AD, Reiman EM, et al. Less activation of the left dorsolateral prefrontal cortex in response to a meal: a feature of obesity. Am J Clin Nutr 2006;84:725–31. https://doi.org/10.1093/ajcn/84.4.725.
[40] Wang J-L, Yang Q, Hajnal A, Rogers AM. A pilot functional MRI study in Roux-en-Y gastric bypass patients to study alteration in taste functions after surgery. Surg Endosc 2016;30:892–8. https://doi.org/10.1007/s00464-015-4288-5.
[41] Smith KR, Papantoni A, Veldhuizen MG, Kamath V, Harris C, Moran TH, et al. Taste-related reward is associated with weight loss following bariatric surgery. J Clin Invest 2020;130:4370–81. https://doi.org/10.1172/JCI137772.
[42] Ten Kulve JS, Veltman DJ, Gerdes VEA, van Bloemendaal L, Barkhof F, Deacon CF, et al. Elevated postoperative endogenous GLP-1 levels mediate effects of roux-en-Y gastric bypass on neural responsivity to food cues. Diabetes Care 2017;40:1522–9. https://doi.org/10.2337/dc16-2113.
[43] Goldman RL, Canterberry M, Borckardt JJ, Madan A, Byrne TK, George MS, et al. Executive control circuitry differentiates degree of success in weight loss following gastric-bypass surgery. Obes Silver Spring Md 2013;21:2189–96. https://doi.org/10.1002/oby.20575.
[44] Baboumian S, Pantazatos SP, Kothari S, McGinty J, Holst J, Geliebter A. Functional magnetic resonance imaging (fMRI) of neural responses to visual and auditory food stimuli pre and post roux-en-Y gastric bypass (RYGB) and sleeve gastrectomy (SG). Neuroscience 2019;409:290–8. https://doi.org/10.1016/j.neuroscience.2019.01.061.
[45] Ochner CN, Kwok Y, Conceição E, Pantazatos SP, Puma LM, Carnell S, et al. Selective reduction in neural responses to high calorie foods following gastric bypass surgery. Ann Surg 2011;253:502–7. https://doi.org/10.1097/SLA.0b013e318203a289.
[46] Ochner CN, Stice E, Hutchins E, Afifi L, Geliebter A, Hirsch J, et al. Relation between changes in neural responsivity and reductions in desire to eat high-calorie foods following gastric bypass surgery. Neuroscience 2012;209:128–35. https://doi.org/10.1016/j.neuroscience.2012.02.030.
[47] van Duinkerken E, Bernardes G, van Bloemendaal L, Veltman DJ, Barkhof F, Mograbi DC, et al. Cerebral effects of glucagon-like peptide-1 receptor blockade before and after Roux-en-Y gastric bypass surgery in obese women: a proof-of-concept resting-state functional MRI study. Diabetes Obes Metabol 2021;23:415–24. https://doi.org/10.1111/dom.14233.
[48] O'Doherty J, Rolls ET, Francis S, Bowtell R, McGlone F. Representation of pleasant and aversive taste in the human brain. J Neurophysiol 2001;85:1315–21. https://doi.org/10.1152/jn.2001.85.3.1315.
[49] King CT, Garcea M, Spector AC. Restoration of quinine-stimulated Fos-immunoreactive neurons in the central nucleus of the amygdala and gustatory cortex following reinnervation or cross-reinnervation of the lingual taste nerves in rats. J Comp Neurol 2014;522:2498–517. https://doi.org/10.1002/cne.23546.
[50] White NM. Some highlights of research on the effects of caudate nucleus lesions over the past 200 years. Behav Brain Res 2009;199:3–23. https://doi.org/10.1016/j.bbr.2008.12.003.
[51] Pak K, Seo S, Lee MJ, Kim K, Suh S, Lee J, et al. Hedonic rating of sucrose is subregionally associated with striatal dopamine transporter in humans. Neuroendocrinology 2021. https://doi.org/10.1159/000517319.
[52] Patkar PP, Hao Z, Mumphrey MB, Townsend RL, Berthoud H-R, Shin AC. Unlike calorie restriction, Roux-en-Y gastric bypass surgery does not increase hypothalamic AgRP and NPY in mice on a high-fat diet. Int J Obes 2019. https://doi.org/10.1038/s41366-019-0328-x.
[53] Soria-Gómez E, Massa F, Bellocchio L, Rueda-Orozco PE, Ciofi P, Cota D, et al. Cannabinoid type-1 receptors in the paraventricular nucleus of the hypothalamus inhibit stimulated food intake. Neuroscience 2014;263:46–53. https://doi.org/10.1016/j.neuroscience.2014.01.005.
[54] Cardinal P, André C, Quarta C, Bellocchio L, Clark S, Elie M, et al. CB1 cannabinoid receptor in SF1-expressing neurons of the ventromedial hypothalamus determines metabolic responses to diet and leptin. Mol Metabol 2014;3:705–16. https://doi.org/10.1016/j.molmet.2014.07.004.
[55] Tremaroli V, Karlsson F, Werling M, Ståhlman M, Kovatcheva-Datchary P, Olbers T, et al. Roux-en-Y gastric bypass and vertical banded gastroplasty induce long-term changes on the human gut microbiome contributing to fat mass regulation. Cell Metabol 2015;22:228–38. https://doi.org/10.1016/j.cmet.2015.07.009.
[56] Tilg H, Zmora N, Adolph TE, Elinav E. The intestinal microbiota fuelling metabolic inflammation. Nat Rev Immunol 2020;20:40–54. https://doi.org/10.1038/s41577-019-0198-4.

[57] Agus A, Clément K, Sokol H. Gut microbiota-derived metabolites as central regulators in metabolic disorders. Gut 2021;70:1174–82. https://doi.org/10.1136/gutjnl-2020-323071.
[58] Panasevich MR, Wankhade UD, Chintapalli SV, Shankar K, Rector RS. Cecal versus fecal microbiota in Ossabaw swine and implications for obesity. Physiol Genom 2018;50:355–68. https://doi.org/10.1152/physiolgenomics.00110.2017.
[59] Yu D, Shu X-O, Howard EF, Long J, English WJ, Flynn CR. Fecal metagenomics and metabolomics reveal gut microbial changes after bariatric surgery. Surg Obes Relat Dis Off J Am Soc Bariatr Surg 2020;16:1772–82. https://doi.org/10.1016/j.soard.2020.06.032.
[60] Liou AP, Paziuk M, Luevano J-M, Machineni S, Turnbaugh PJ, Kaplan LM. Conserved shifts in the gut microbiota due to gastric bypass reduce host weight and adiposity. Sci Transl Med 2013;5. https://doi.org/10.1126/scitranslmed.3005687. 178ra41.
[61] Park S-K, Kim M-S, Roh SW, Bae J-W. Blautia stercoris sp. nov., isolated from human faeces. Int J Syst Evol Microbiol 2012;62:776–9. https://doi.org/10.1099/ijs.0.031625-0.
[62] Gao Z, Yin J, Zhang J, Ward RE, Martin RJ, Lefevre M, et al. Butyrate improves insulin sensitivity and increases energy expenditure in mice. Diabetes 2009;58:1509–17. https://doi.org/10.2337/db08-1637.
[63] Zizmare L, Boyle CN, Buss S, Louis S, Kuebler L, Mulay K, et al. Roux-En-Y gastric bypass (RYGB) surgery during high liquid sucrose diet leads to gut microbiota-related systematic alterations. Int J Mol Sci 2022;23:1126. https://doi.org/10.3390/ijms23031126.